2013

Human injury model for small unmanned aircraft impacts

Civil Aviation Safety Authority

Civil Aviation Safety Authority / Monash University

12/23/2013

Revisions

Date	Name	Notes
14.10.2013	Alexander Radi	Initial version 0.1
11.11.2013	Alexander Radi	Appendix B added (cutting injuries discussion)
11.11.2013	Alexander Radi	Appendix C added (7kg limit justification)
19.12.2013	Alexander Radi	Abstract rewritten as executive summary
20.12.2013	Alexander Radi	Text streamlined, bibliography added
23.12.2013	Alexander Radi	Grammar corrections

Executive summary

This report describes an injury prediction model for the impact of small Remotely Piloted Aircraft (RPA) into a person on the ground. The model provides estimates of injury severity as a function of the RPA's mass and impact velocity. One of the goals is to determine a 'non-lethal' RPA mass for purpose of drafting air traffic regulations for the rapidly developing civil RPA market.

A literature review of existing injury models from the automotive and defence industries suggested using the Blunt Criterion (BC). This empirical model predicts the severity of blunt trauma injuries (impact without skin penetration) based on the impacting projectile's kinetic energy and impact diameter. In the present study, impacts into the thorax (chest) and head are considered; modifications to the BC for the latter case are discussed. In accordance with other studies, serious injury (AIS=3) is defined as the maximum acceptable injury severity.

The model results indicate a higher sensitivity for head injuries than for injuries to the thorax. The impact into the thorax with a 2kg object at 10m/s (20kts) is survivable with serious injuries. The model predicts the absence of serious head injuries (skull fracture) for an RPA mass under 2kg and impact velocities below 7.5m/s (15kts). In each case a certain minimum 'roundness' of the impacting part is required (at least 10cm impact diameter).

Due to the complex geometry of the RPA and the non-trivial biomechanics of the human body, major simplifications and assumptions had to be made during the adaptation of the BC. The current model ignores the collision dynamics and the RPA material's frangibility and elasticity, making its predictions over-restrictive. On the other hand, certain injury types like brain concussion, heart arrest or neck injury are not considered. Overall, the biggest source of uncertainty results from the application of the BC—which was developed for small projectiles of 20–50mm in diameter and 50–100g mass—to full-scale RPAs.

1 Table of Contents

2 Introduction

2.1 Objectives

This report presents the findings of a study carried out by Alexander Radi M.Sc.[1] during a four months research internship at CASA (Canberra). The aim of the study is to provide the Standards Development branch at CASA with an assessment of injury severity from the impact of small Remotely Piloted Aircraft (RPA) into a person on the ground. Of particular interest are combinations of RPA mass and impact velocity which cause non-severe injuries.

2.2 Background

Recent media reports of small RPAs colliding with structures and hitting—or just missing—people on the ground exemplify the potential danger of operating these machines in populated areas.[2][3][4] Not every collision results in serious injuries, implying a minimum RPA mass below which the RPA can be considered as harmless (causing non-severe injuries or fatality upon impact). Currently, there are no guide lines on this limit, which can serve as an appropriate cut-off point for prescriptive regulation, whereby less prescriptive industry / professional standards of practice can be adopted.

Currently, CASA imposes operational restrictions on small RPAs weighing more than 100 grams, because it does not have sufficient data on the potential injury that could be caused to people on the ground resulting from a blunt ballistic impact. It is reasonable to assume that the injury potential correlates to the impact kinetic energy, characteristic diameter of RPA's part contacting the body, attitude on impact, and the frangibility of the unmanned airframe. The present study attempts to examine the influence of these parameters on the expected injury potential. Due to the complexity and the time limitation of the project, simplifying assumptions had to be made regarding the impact attitude and frame frangibility.

2.3 Method

The review of available literature concentrated on online medical journals, such as:

- *The Journal of Trauma Injury, Infection, and Critical Care*
- *Medicine & Science in Sports & Exercise*
- *Journal of Biomechanics*
- *International Journal of Legal Medicine*
- *Forensic Science International,*

and on journals from the field of automotive crashworthiness:

- *International Journal of Crashworthiness*
- *Stapp Car Crash Journal*
- *Accident Analysis and Prevention.*

The goal of the review was to find suitable and validated human injury criteria and models, which could be adapted to the present task with minimum modifications. The selected model (the 'Blunt

[1] Ph.D. candidate Aerospace Engineering at Monash University, Melbourne
[2] http://www.smh.com.au/nsw/mystery-drone-collides-with-sydney-harbour-bridge-20131004-2uzks.html
[3] http://abclocal.go.com/wabc/story?id=9270668
[4] http://rt.com/usa/virginia-bull-run-drone-002/

Criterion') describes blunt trauma injuries from small ballistic projectiles, such as used by law enforcement agencies in non-lethal weapons. This model is based on animal and human cadaver experiments and predicts various levels of injury severity beyond a simple life/death distinction. The deciding advantage of the selected model over other injury criteria (e.g. from the automotive sector) is the use of the projectile's physical properties for injury prediction, instead of the biomechanical response of the body during impact, such as forces or accelerations.

Once a suitable model had been found, it was modified to describe large-object impacts, such as RPAs. For thorax impacts, these modifications ware adopted from previous literature; for head impacts, original modifications had to be developed based on geometry and basic physical principles.

The extension of the existing model to large-object impacts made the validation of the results difficult due to the lack of matching experiments. The results are compared against sports accidents (cricket, baseball) and to head injuries during falls on rigid flat surfaces. Limitations of the model due to neglected effects and uncertainties of the input parameters were identified.

2.4 Study structure

The present document shortly discusses the rationale behind the selected model in sections 3 and 4. Sections 5 and 6 contain the mathematical details of the model and the implemented modifications for chest and head impact, respectively. The model results and partial validations are presented in section 7. It is important to consider the limitations of the model which are discussed in section 8. The conclusions of the study and recommendations regarding the design, weight and velocity limits of small RPAs are summarized in section 9.

3 Physical background

3.1.1 Perfectly inelastic collision

The underlying assumption of the proposed injury model is the perfectly inelastic collision, as shown in Figure 1. Prior to the impact (situation *I*), the impacting body of mass M_1 moves at velocity V_1 towards the (for the sake of simplicity) stationary body 2 of mass M_2. After the impact (situation *II*), both objects move as a combined body of mass M_1+M_2 at the resulting velocity V_{II}. This situation represents a human (or human part, such as the head) of mass M_2 being impacted by an RPA of mass M_1 at velocity V_1.

Two physical quantities describe this process: The linear momentum p and the energy E. Of interest for the injury prediction is the kinetic energy of the impacting object $E_{kin,I}$. After the impact, the smaller fraction of this energy exists in form of the kinetic energy of the two combined masses ($E_{kin,II}$), which move now at V_{II}. The remaining energy has been transformed into deformation energy E_{def}, deforming the two bodies. Assuming that the impacting RPA structure is rigid, it is the whole of E_{def} that 'deforms' the human body, causing the actual injuries.

As the impactor mass M_1 increases relative to the target mass M_2, a smaller fraction of the kinetic energy is transformed into deformation energy (although the absolute E_{def} increases!), and the target body is accelerated to higher velocities (Figure 2). This leads to high accelerations when a comparably small body part (e.g. head) is hit by a heavy object. Even in the absence of external injuries, these high accelerations can result in a brain concussion or neck injuries (think of a soccer ball hitting the head at high velocity). This type of injury will be excluded in the present model. Yet, if energy absorbing materials are used on the RPA, injuries from high accelerations become more likely.

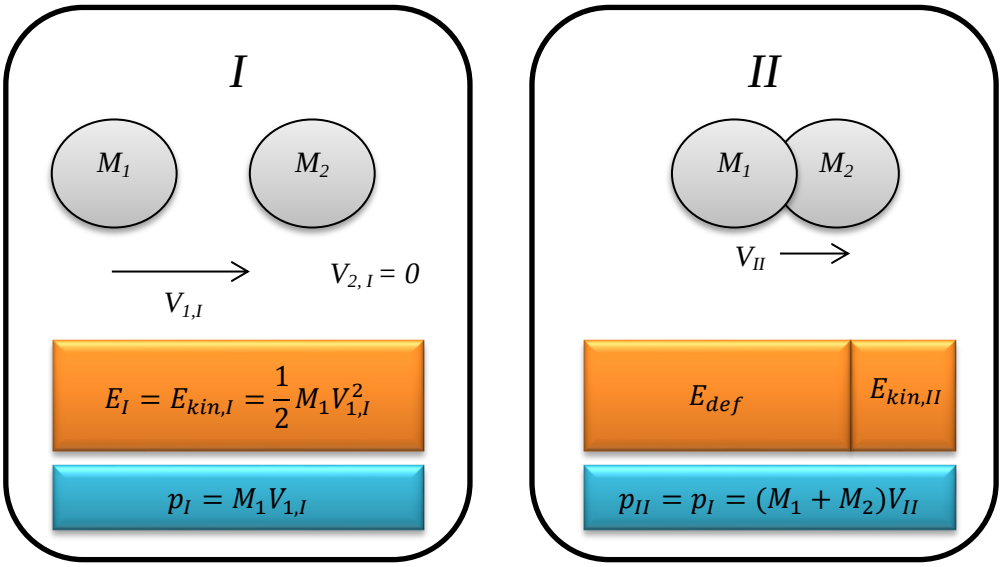

Figure 1: Conservation of energy *E* and linear momentum *p* in a perfectly inelastic collision.

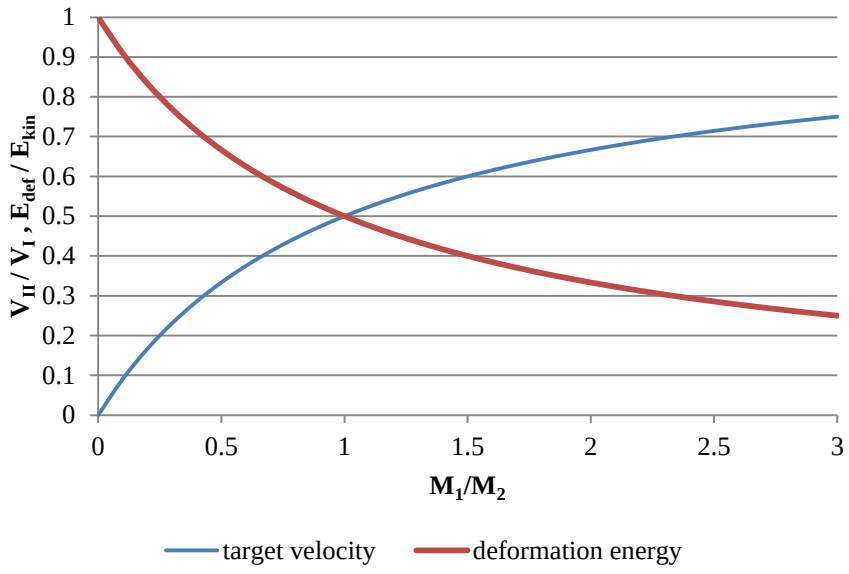

Figure 2: Resulting target velocity and the deformation energy fraction as a function of impactor mass M_1.

4 Existing Injury prediction models

Two industries employ impact injury prediction models: the automotive and the defence industry.

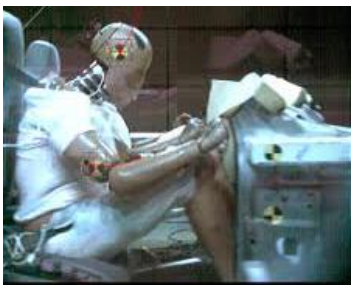

Figure 3: Automotive crash testing

The automotive industry is concerned with predicting and reducing injuries in car, motorbike and pedestrian accidents. Most injuries result from the body, or body parts, impacting other objects, such as dashboards, seats or windscreens (direct interaction). Special cases are injuries due to high accelerations without impact, such as neck injuries ('whiplash'), or fractured ribs due to seatbelt restraint (indirect interaction).

The defence industry deals with inflicting or preventing injuries from high kinetic energy objects, such as projectiles or debris. Within this field, a rather new technology of 'less-lethal kinetic energy munitions' emerged in the last 20–30 years. These munitions are designed to impact the body without producing severe or fatal injuries and are used by law enforcement agencies in riot control.

Figure 4: Russian non-lethal weapon "Wasp"

Although blunt impact injuries (injuries without skin penetration) are important in both fields, the physics involved and the methods of predicting these injuries are quite different. In an automotive crash scenario, the impacting body mass is in the order of 10–100kg, and moves at velocities up to 20m/s (high momentum). A less-lethal projectile weights up to 200g and moves at a maximum velocity of 200m/s. The resulting low momentum leads to extremely short impact durations of 2–5ms and high peak forces (compared to 10–30ms in automotive crashes). The momentum determines the injury biomechanics: crush & shear in the former, and the viscous mechanism in the latter case (Widder, et al., 1997) (Viano, et al., 1992). The velocity and mass of small RPAs reside somewhere between these two scenarios (5–20m/s; 0.5–20kg).

Unfortunately, the methods employed in automotive crash testing make this large pool of data unsuitable for the present study. Figure 5 shows the two different approaches used by the two industries: The automotive industry measures the forces, moments and accelerations of the crash dummy during the impact. These time-resolved measurements are compared to empirical limits to predict the injury severity. These limits were obtained from experiments with animal or human cadavers, in-vivo measurements or by comparison with accident statistics. Such data bases do not exist for RPA impacts, and it is not possible to calculate forces and accelerations from energy or momentum considerations alone.

The less-lethal munitions injury criterion, on the other hand, is directly based on the energy content of the projectile. The link between the energy level and the injury severity is formed by the Blunt Criterion (BC).

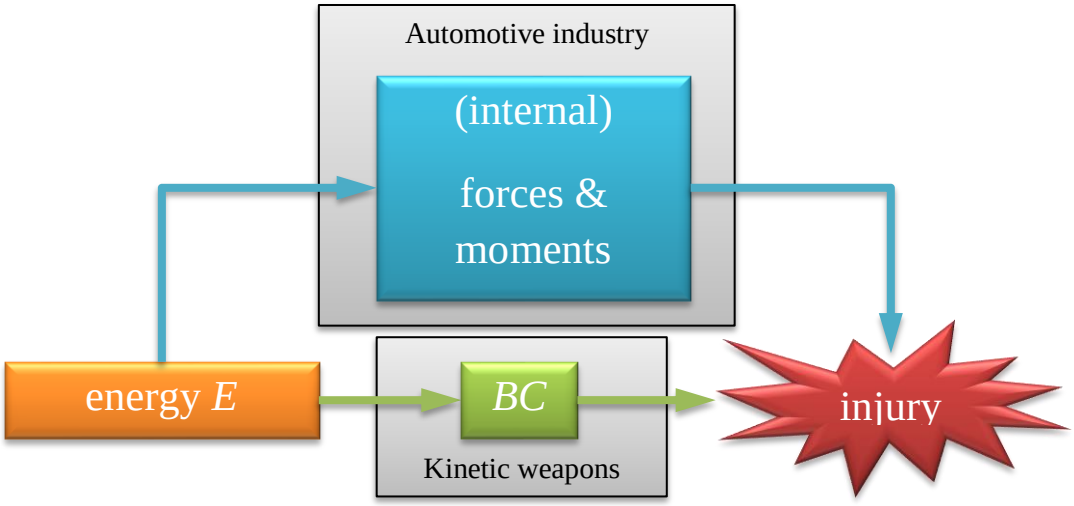

Figure 5: Criteria used to predict the injury severity. The automotive industry relies on measuring the forces and moments in the crash dummy, while the less-lethal kinetic wepons are assessed via the the Blunt Criterion (BC) using the projectile energy *E* directly.

4.1 The Blunt Criterion

The BC has been extensively researched for blunt impacts, and is based on research conducted by the U.S. military in the 1970s. This research was commissioned to collect and correlate all existing blunt impact injury data of the thorax (Clare, et al., 1975). The resulting five parameter model is defined as follows (Sturdivan, et al., 2004):

$$BC = \ln\left(\frac{\frac{1}{2}MV^2}{W^{1/3}TD}\right) \qquad 1$$

where M[kg] is the mass, V[m/s] is the velocity and D[cm] is the diameter of the projectile, W[kg] is the mass of the struck body and T[cm] is the thickness of the body wall. Figure 6 shows the impact situation and parameters.

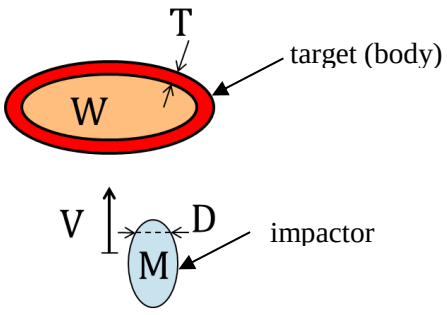

Figure 6: Physical parameters used for the Blunt Criterion.

The BC accounts for the current consensus that the impact energy alone is not an accurate enough predictor of injury. The BC relates the projectile's energy to the capacity of the body to tolerate the inflicted tissue damage. As the equation shows, the numerator represents the kinetic energy of the projectile. The denominator is a semi-empiric expression of the capacity of the body (or body part) to absorb this energy. The scaling takes into account the body mass and the thickness of the protective

wall (ribs, soft tissue) around the vulnerable organs. In addition, the diameter of the projectile provides a scaling for the contact area during the transmission of impact energy.

This criterion was originally developed for chest impacts, and has been extended to head impacts only recently (Raymond, et al., 2009). The present study will use a modified version of this criterion to predict injuries to the thorax and head. Neck injuries will be excluded from the present study as no energy based criterion—equivalent to the BC—exists for this body part, and the results from automotive crash testing are not usable due to reasons discussed above. Furthermore, injuries to the body extremities will be treated as non-life-threatening and thus ignored.

4.2 Abbreviated Injury Scale (AIS)

First, a quantitate measure of injury severity needs to be introduced. The Abbreviated Injury Scale (AIS) is one of the most common anatomic scales for traumatic injuries, and is being used internationally. The AIS is an anatomical-based coding system created by the Association for the Advancement of Automotive Medicine to classify and describe the severity of specific individual injuries. It represents the threat to life associated with the injury, rather than the comprehensive assessment of the severity of the injury. The scale ranges from 1 to 6 (Table 1), where 1 is a minor injury, seldom requiring medical treatment, while 6 stands for 100 per cent probability of death. Any injury greater than AIS=3 is considered life-threatening.

AIS code	Injury	Example	AIS % prob. of death
1	Minor	superficial laceration	0
2	Moderate	fractured sternum	1–2
3	Serious	open fracture of humerus	8–10
4	Severe	perforated trachea	5–50
5	Critical	ruptured liver with tissue loss	5–50
6	Maximum	total severance of aorta	100

Table 1: Abbreviated Injury Scale (from Wikipedia[5])

[5] http://en.wikipedia.org/wiki/Abbreviated_Injury_Scale

5 Impact into the thorax

As seen in Equation 1, the tolerance to blunt impact depends on the human body mass. It is customary to assume 50kg for the 5th percentile female, 75kg for the 50th percentile male and 100kg for the 95th percentile male. In the present study, the injury severity will be calculated for the most vulnerable group, the 5th percentile female with body mass $W_B = 50\text{kg}$.

5.1 Effective mass of the thorax

In the original formulation of the BC, the mass of projectile was assumed to be much smaller than the body mass. This means that the impact stops the projectile without accelerating the body. Thus, all kinetic energy of the projectile is transformed into deformation energy, which constitutes the numerator in Equation 1. The mass of a small RPA, as considered in the present study, ranges from 0.5–20kg, which is similar or larger than the body part mass (thorax, head). This makes it necessary to consider both, the deformation energy E_{def} and the remaining kinetic energy in the body/RPA after impact, as shown in Figure 1. As not the whole body is accelerated during impact, *the effective mass* W_{BP} (Table 2) of the struck body part will be used for the calculation of E_{def} (Sturdivan, et al., 2004). This is the mass that would move relatively independent of adjacent body parts after an impact by a projectile of comparable mass. The deformation energy is computed as

$$E_{def} = \frac{1}{2}\mathrm{M}\,\mathrm{V}^2\left(1 - \frac{M}{M + W_{BP}}\right). \qquad 2$$

For example, for a M=2kg RPA impacting a W_B =75kg heavy person at V=20m/s in the thorax (W_{BP} =0.21* W_B), 89 per cent of the total kinetic energy (400J) is inflicted onto the body as deformation energy.

Body Part	Men & Women [%]
Head	N/A
Arm	7
Thorax	21
Midabdomen	21
Pelvis	20
Leg	33

Table 2: Relative body part mass W_{BP} for injury prediction. (Sturdivan, et al., 2004)

Using Table 2, the effective mass of the thorax will be set to:

$$W_{Th} = 0.21 * 50\text{kg} = 10.5\text{kg} \qquad 3$$

5.2 Body wall thickness

The body wall thickness T depends mainly on the body mass. (Sturdivan, et al., 2004) provide the following formula based on laboratory data:

$$T = kW^{1/3}, \qquad 4$$

with $k = 0.59$ for females and $k = 0.711$ for males. The value for a 50kg female thorax is $T_{Th} \approx 2.2\text{cm}$.

5.3 Impact diameter

The second modification of the original model consists of an adjustment of the diameter D. It is the area of contact, represented by D, which scales the amount of tissue available to absorb the impact energy. When a small, blunt object is involved, the area of contact is just the cross-sectional area of the object. As the size of the object increases, the area of contact is determined by the curvature of the object.

(Sturdivan, et al., 2004) suggested a spherical shape of diameter D' for simplicity. While impacting, the object pushes into the body, displacing the soft tissue, as seen in Figure 7. If the beginning of injury is considered to be the point at which the sphere has pushed the distance equivalent to the body wall thickness T, then geometry gives the area of contact A:

$$A = \pi T(D' - T); \;\; D' > 2T. \qquad 5$$

The *effective diameter* D to be used for the thorax in Equation 1 is:

$$D_{Th} = 2\sqrt{A/\pi}. \qquad 6$$

It will be assumed that D' is the local diameter of the RPA part striking the body. Equations 5 and 6 will be used for D' larger than $2T_{Th} \approx 5$cm.

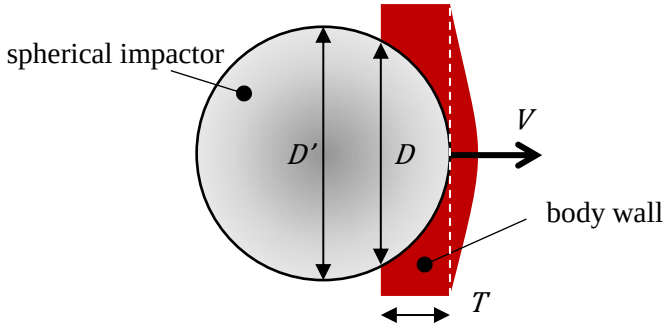

Figure 7: Body wall during impact with a spherical object of diameter $D'>2T$. Note the 'effective diameter' D.

5.4 Experimental injury data

The BC uses experimental data to relate the deformation energy to injury severity. These data had been obtained by striking animal or human cadaver with impactors and grading the autopsy results according to the AIS. Naturally, the correlation shows a large spread, with particularly large differences between cadaver and in-vivo experiments. For the present study, it is suggested to use the data compiled by (Sturdivan, et al., 2004), who report

$$BC_{Th} = 0.48 \qquad 7$$

for a 50 per cent probability of sustaining a serious, but not life threatening AIS=3 injury of the thorax. The probabilities of sustaining other injury severities at BC=0.48 are listed in Table 3.

AIS	1	2	3	4	5	6
probability	86.2%	79.7%	50.0%	16.7%	0.8%	0.1%

Table 3: Probability of injury severity at BC=0.48 based on data from (Sturdivan, et al., 2004).

6 Impact into the head

Head injury estimates will be based on the study by (Raymond, et al., 2009), who adopted the BC to the physiology of the skull. The results were derived from experiments consisting of impacting human cadaver heads with ballistic projectiles ($M = 0.1$kg, $D = 3.8$cm) at velocities 20 and 35m/s. Skull fracture, which is equivalent to AIS=3 and which leads to a mortality rate of 11 per cent (Raymond, 2008), was defined as the injury criteria. The experiments showed that a 50 per cent risk of skull fracture is represented by

$$BC_H = 1.61. \tag{8}$$

This value will be used in the present study as the injury threshold.

The following chapter discusses the necessary adjustments to the parameters in the BC formula (Equation 1), which affect the body wall thickness T, the body part mass W and the effective diameter D (note that (Raymond, et al., 2009) used the head mass as the body part mass as W in Equation 1).

6.1 Effective mass of the head

The post-mortem heads used by Raymond (2009) were detached from the body, such that only absolute head masses were provided (with an average of 3.4kg). The *effective* head mass required for the calculation of E_{def} can be determined through in-vivo free vibration experiments, as performed by (Lim, 2005):

$$W_H = 6\text{kg}. \tag{9}$$

6.2 Wall thickness

The body wall thickness T of the head consists of the skull thickness and the thickness of the surrounding soft tissue. (Raymond, et al., 2009) report a value of

$$T_H = 1.3\text{cm}. \tag{10}$$

6.3 Impact diameter

The biggest difficulty in adopting the BC to head impacts lies in the determination of the effective diameter D. For the thorax, the impact geometry consisted of a spherical object hitting a flat surface (chest), which made the determination of D straightforward. (Raymond, et al., 2009) impacted cadaver heads with flat-faced projectiles, which known diameter could be directly used in Equation 1. In the present study, it must be assumed that the impacting RPA part has a certain curvature defined by its local diameter D'. The varying local curvature of the head makes the collision geometry even more complex.

As a first simplification, the skull shape will be approximated by a sphere of diameter D_{Sk}=18cm. Thus, the geometry under consideration is a spherical impactor depressing a sphere-shaped head to a depth of x_{dep} (Figure 8). D is the imprint diameter left in a soft sphere of diameter D_H after collision with a rigid sphere of diameter D'. Depending on the experimental conditions and impacting velocities, depression values x_{dep} =7–15mm prior to fracture have been reported (Yoganandan & Pintar, 2004). In the present model, the average value from (Raymond, 2008) will be used:

$$x_{dep} = 0.9\text{cm}. \quad (11)$$

The contact diameter (or equivalently the area A) between the two spheres will be determined as follows: Based on the idealized skull diameter of D_{Sk}=18cm, the range of impactor diameters D' can be divided into 3 groups:

1. $T_H < D' \ll D_{Sk}$
2. $D' \approx D_{Sk}$
3. $D' \gg D_{Sk}$

The impactor dimensions of the first group are much smaller than the skull size, being in the order of the wall thickness T_H. The second group consists of impactor sizes comparable to the skull size. And the third group comprises of objects much larger than the head size, with the limiting case of the head hitting a flat surface ('flat plate limit' $D' \to \infty$).

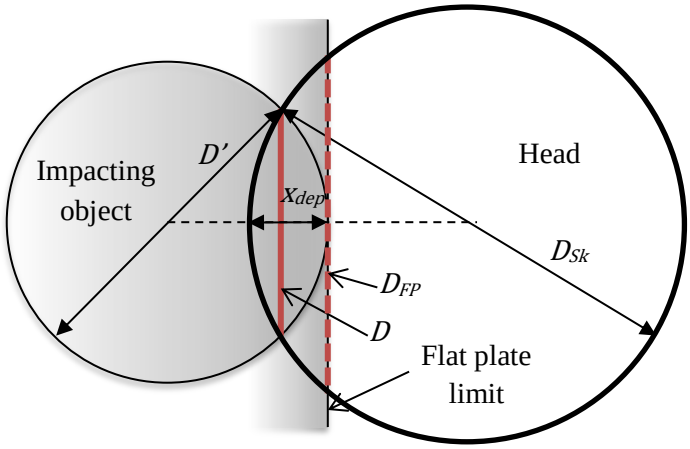

Figure 8: Impact geometry and dimensions during head impact.

The impactor size and the depression depth x_{dep} determine the contact area available for the transmission of the impact energy. It was shown in experiments that different contact areas can result in different fracture mechanisms of the skull (Raymond, 2008). Three failure mechanisms exist, as shown in Figure 9: Small objects with an area less than approximately 6cm^2 (<1 inch^2) are likely to penetrate the skull, leaving a hole of the size of the object itself. Larger impactors break and depress a bone section larger than the impactor area; for this case the BC was validated by (Raymond, et al., 2009). The limiting case of the impact of the head on a flat surface (or a big object) will result in radial propagation of linear fractures through the bone. These three failure modes result from different bone-internal stress responses. Generally, the skull can tolerate larger impact forces for larger contact areas.

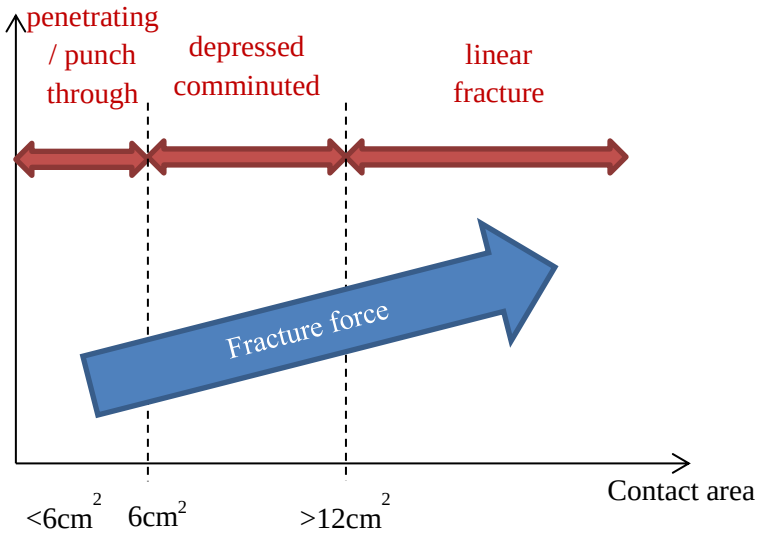

Figure 9: Different skull failure mechanisms as a function of the contact area between the impactor and head. (Raymond, 2008)

Not all these scenarios will (and need to) be considered in the present model. At the lower limit, the punch-through case will be ignored, with the assumption that the RPA does not possess sharp protrusions. The existence of such protrusions is likely to lead to skin-penetrating (and skull-penetrating) injuries, which would require a separate injury model.

Mid-sized impactors ($2T < D' \approx D_{Sk}$) will be treated with the BC, extended for spherical impactor shapes. Rearranging Equation 1 gives the effective diameter:

$$D = \frac{E_{def}}{W^{1/3} T_H e^{BC}} = \frac{\frac{1}{2} M V^2}{W^{1/3} T_H e^{BC}} \left(1 - \frac{M}{M + W_H}\right), \qquad 12$$

where W_H is the effective mass of the head, W=3.4kg is the head mass used by (Raymond, et al., 2009) and M and V are the mass and velocity of the impacting RPA, respectively. Contact diameters larger than D reduce the risk of fracture by distributing the deformation energy over a larger contact area. Given the contact diameter D for given impactor mass and velocity (kinetic energy), the minimum allowable impactor diameter D' can be calculated. Given the depth of the depression x_{dep}, the impactor diameter is

$$D' = \frac{D^2}{4 x_{dep} \left(1 - \frac{D - 2T_H}{D_{FP} - 2T_H}\right)} + x_{dep} \left(1 - \frac{D - 2T_H}{D_{FP} - 2T_H}\right). \qquad 13$$

The calculation is based on the radius of a three-point arc, as derived in Appendix A.

Equation 14 already incorporates the upper limit of a large-sized impactor, equivalent to an impact with a flat plate. This case determines the variable D_{FP}, which is the diameter of the contact area A_{FP} between a flat surface and a soft sphere depressed by x_{dep}. Accordingly, D' goes to infinity when D approaches D_{FP}. This means that as the impactor mass and/or velocity increases, the increased deformation energy needs to be distributed over a larger contact area to keep the injury severity constant. The collision geometry imposes an upper limit on the available contact area A_{FP}, beyond which not even a flat plate provides enough contact surface to spread the energy to prevent injury.

This situation provides a natural limit on the maximum deformation energy, which can be inflicted by a flat-plate impact. This scenario can be used as a 'cut-off' point for regulatory purposes, the argument being: "Above this kinetic energy (mass/velocity combination), the probability of a serious head injury (skull fracture) is above the 50 per cent threshold, even if the RPA impacts with one of its flat sides." When impacting with a curved surface, the tolerable kinetic energy is even lower. The model predicts 76 Joules as the maximum tolerable deformation energy during an impact with a flat surface. The energy density of the contact area is approximately 1.6J/cm^2. The validity of these results will be discussed in section 7.3.

7 Results

7.1 Expected velocity range

The impact velocity plays a dominant role for the prediction of injury severity. The expected velocity values are determined by the impact scenario. (Haddon & Whittaker, 2004) suggest 2 possibilities:

1. *Unpremeditated descent scenario (UDS)*, in which the RPA is under control but unable to maintain altitude, and in which the impact velocity is 30 per cent over minimal (i.e., stall airspeed). The expected velocity range is 10–15m/s for a small RPA.
2. *Loss of control scenario (LCS)*, with the RPA impacting at a velocity 40 per cent higher than maximum airspeed attainable in level flight. The expected velocity lies above 30m/s for small RPAs.

Another scenario is the *uncontrolled descent*, in which the RPA reaches terminal speed based on its drag coefficient (this case is similar to the LCS). (Magister, 2010) showed that this velocity is reached by a small RPA during a descent from an altitude of just 60m AGL, and can be expected to be approximately 30m/s.

Figure 10 exemplifies the high kinetic energies created by these velocities. Although pure kinetic energy has been shown to be not sufficient for accurate injury prediction, rough estimates of expected injury severity based on E_{kin} are included in this figure (Frank, 2012). Considering energies of 40–120J as dangerous, and >120J as causing severe damage to humans, an impact of a small RPA with a mass of just 0.5kg can be considered as potentially deadly at V>27m/s. The velocities involved in LCS and the terminal velocity scenarios are considerably above the 'severe damage' threshold of 120J. For illustration: 120J is equivalent to a mid-size hammer (0.5kg) dropped from the eighth floor (24.5m drop height, 22m/s at impact). Focusing on kinetic energies below 120J, and limiting the RPA mass to 0.5–20kg, the velocity range of interest for the present study becomes 3–22m/s (6-40kts) (marked by the dashed box in Figure 10).

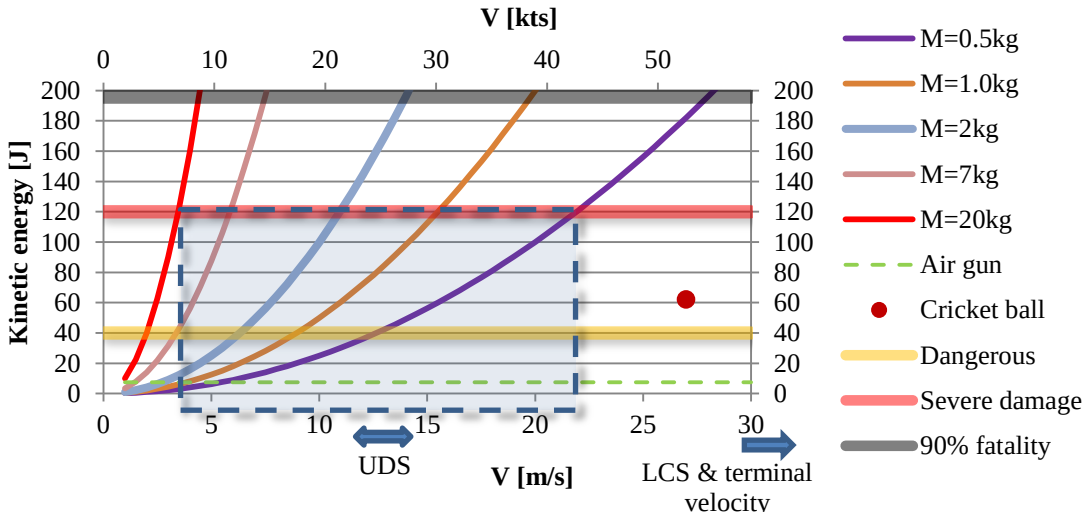

Figure 10: Kinetic energy as a function of RPA mass and velocity. Rough injury estimates are shown as horizontal lines. The present study considers the parameters within the dashed box.

7.2 Chest impact

AIS=3 is chosen as the highest acceptable injury severity (AIS=3: serious injury, such as rib fracture or fracture of the sternum). Intuitively, higher RPA mass and velocity increase the injury severity, while a bigger object size reduces the injury severity. Object diameters up to D'=30cm will be considered, which is approximately the chest width.

Figure 11 shows the model results as combinations of M, D' and V, which are divided into acceptable and unacceptable regions. To the *left* of each line (which represent a given impact velocity), any combination of M and D' results in an injury below AIS=3, which is the acceptable region. To the *right* of each line, the injury severity is unacceptably high. For example, a ten-pin bowling ball (M=7kg, D'=21cm) will cause severe injuries if hitting the chest at a velocity of 7.5m/s, as this mass-velocity combination lies to the right of the 7.5m/s line. The injuries will be acceptable, if being hit at a velocity of 5m/s, as this mass-velocity combination lies to the left of the 5m/s line. These two velocities are equivalent to dropping the ball from heights of 2.9m and 1.3m, respectively. The kinetic energies are 200J and 87J, respectively (the inflicted deformation energies are lower).

It should be kept in mind, that the limits drawn in Figure 11 are not a life/death distinction. The lines represent serious injury potential with 1per cent probability of death.

When applied to unmanned aircraft: A 2kg RPA hitting the thorax at 10m/s (20kts) needs a minimum part diameter of 15cm to keep the injury potential in the acceptable range. At 15m/s, an unrealistically large diameter (>30cm) would be required to prevent severe injuries.

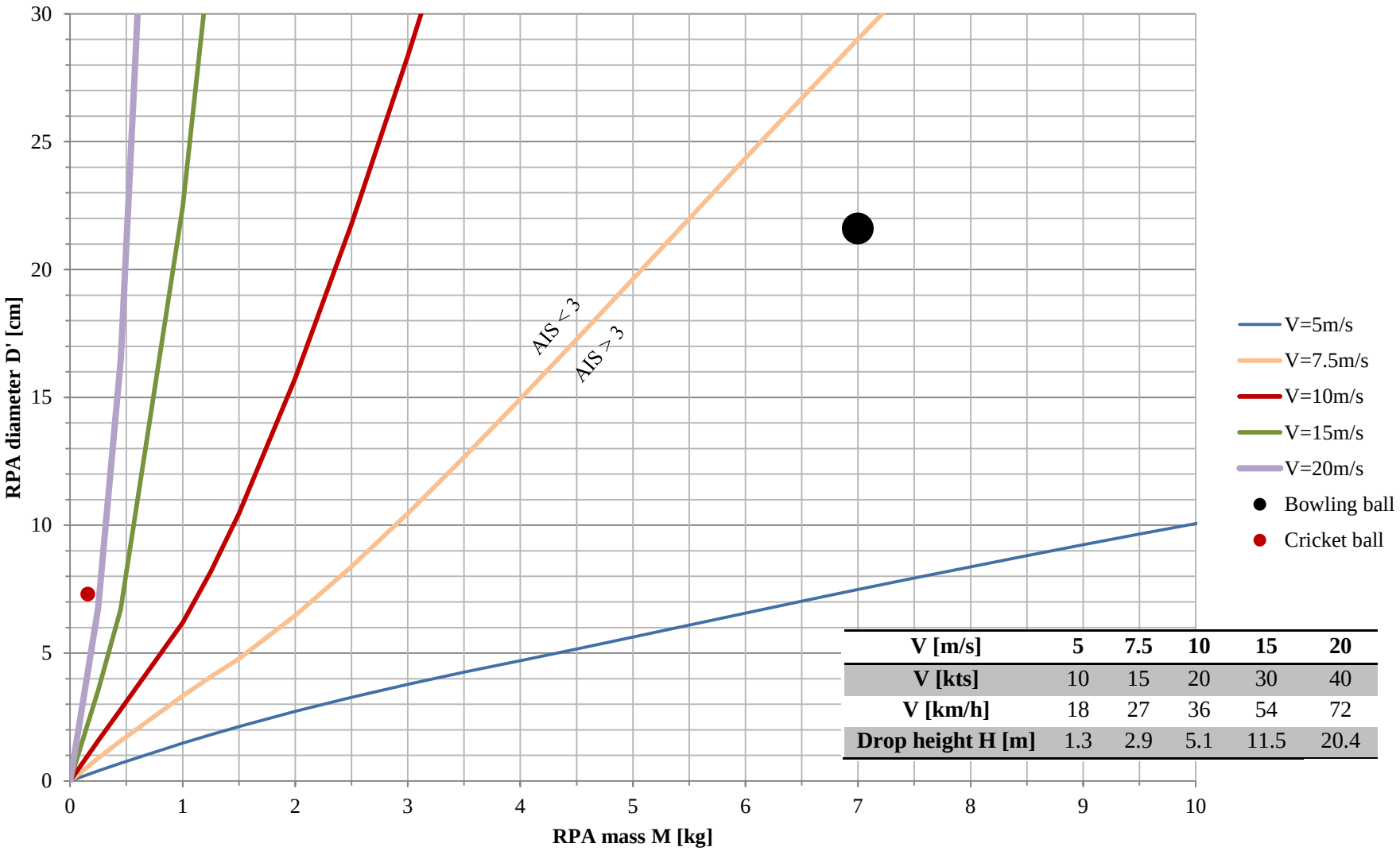

V [m/s]	5	7.5	10	15	20
V [kts]	10	15	20	30	40
V [km/h]	18	27	36	54	72
Drop height H [m]	1.3	2.9	5.1	11.5	20.4

Figure 11: 50% probability of serious injury (AIS=3) of the thorax as a function of RPA impact velocity *V*, mass *M* and diameter *D'*.

7.3 Head impact

BC=1.61 (representing 50 per cent probability of skull fracture) will be used as the limit for the head injury severity. Figure 12 shows the model results for head impacts: To the left of the solid lines, the injury severity is acceptable, while to the right of the lines skull fracture should be expected for a given impactor size and mass. The dividing lines are steeper than in the thorax impact scenario, implying a higher sensitivity for head injury. For head impacts, the impactor size is not limited to 'mid-sized' objects any more, and the limit of an infinite diameter—which is equivalent to a flat surface—needs to be considered. The dashed vertical lines in Figure 12 are such 'flat plate limits'. They represent the maximum impactor mass for a given velocity that would inflict just the critical injury (50 per cent probability of skull fracture) when the impactor hits the head with its flat side. Any mass higher than this limiting value will lead to head fracture regardless of the contact area / impactor diameter. These limits are equivalent to 76J deformation energy.

A cricket ball will be used for a rough validation of the results for small object impacts. According to the model, a 0.16kg cricket ball becomes dangerous at velocities above 25m/s (100km/h), which is equivalent to >50J. The lower energy threshold compared to the flat-plate limit is a consequence of the small ball size (small contact diameter D). The fastest recorded cricket delivery was 160km/h, with velocities of above 100km/h being the norm. This means that such impacts are very likely to lead to severe or fatal injuries. Table 4 shows that cricket deaths have occurred in the past, but were not directly related to the ball impact. The exception is case 6, where the impact caused an internal haemorrhage; but still no skull fracture was reported. In this case, a rebound of the ball was reported, which reduced the impact energy. This data suggest that the model produces conservative predictions for small object impacts.

	Year	Name	Impact to	Cause of death
1	1870	George Summers	head	abscess in lung
2	1958	Abdul Aziz	chest	heart condition?
3	1971	Roger Davis	head	heart arrest
4	1960s	Nariman Contractor	back head	(survived, retired)
5	1993	Ian Folley	eye	heart attack
6	1998	Raman Lamba	forehead	internal bleeding
7	2009	umpire	head	(not known)

Table 4:Cases of severe or fatal cricket ball injuries (from Wikipedia)

For the large-object limit (the vertical dashed lines), the model predicts 76 Joules as the maximum tolerable deformation energy during an impact with a flat surface. The energy density of the contact area is approximately 1.6J/cm^2. There have been numerous experiments of head impacts on a rigid flat surface, and Table 5 suggests that fractures can be expected for E_{def} > 100–200J. The critical value of the proposed model is at the lower limit of this range and provides a large margin of safety. On the other hand, the R.C.C. Supplement to standard (321-00, 2000) estimates a 10 per cent probability of fatality (this is similar to an AIS=3 injury) from a 51J impact. Recent computer simulations of head impacts onto flat rigid surfaces show skull fractures only for impact velocities above 6.0-6.5m/s, which is equivalent to 80–95J for a head mass of 4.5kg (Thollon, et al., 2013) (Hamel, et al., 2013). In conclusion, it is reasonable to assume a survivable AIS=3 head injury for deformation energies E_{def} <100J in case of a flat surface impact, which is in agreement with the current model.

E_{def}	Fracture	Source
37	No	Advani 1975
76	**50%**	**model**
104	No	Advani 1975
110	Yes	Allsop 1991
>200	Yes	McIntosh 1993
230	Yes	Stalnaker 1977
260	Yes	Stalnaker 1977

Table 5: Comparison of the model's maximum tolerable deformation energy during an impact with a rigid flat surface with experimental data.

A 2kg RPA lies between the solid and dashed lines of V=10m/s (20kts). This means that the injury severity is dependent on the diameter contacting the body. While an impact with a flat surface is likely to be tolerable, the contact with any rounded surface is predicted to lead to skull fracture. A lower velocity of 7.5m/s, on the other hand, is not critical for RPA part diameters above approximately 10cm.

These values should be considered as rough estimates, due to the high sensitivity of the model to the input parameters (such as head diameter D_H and depression depth x_{dep}).

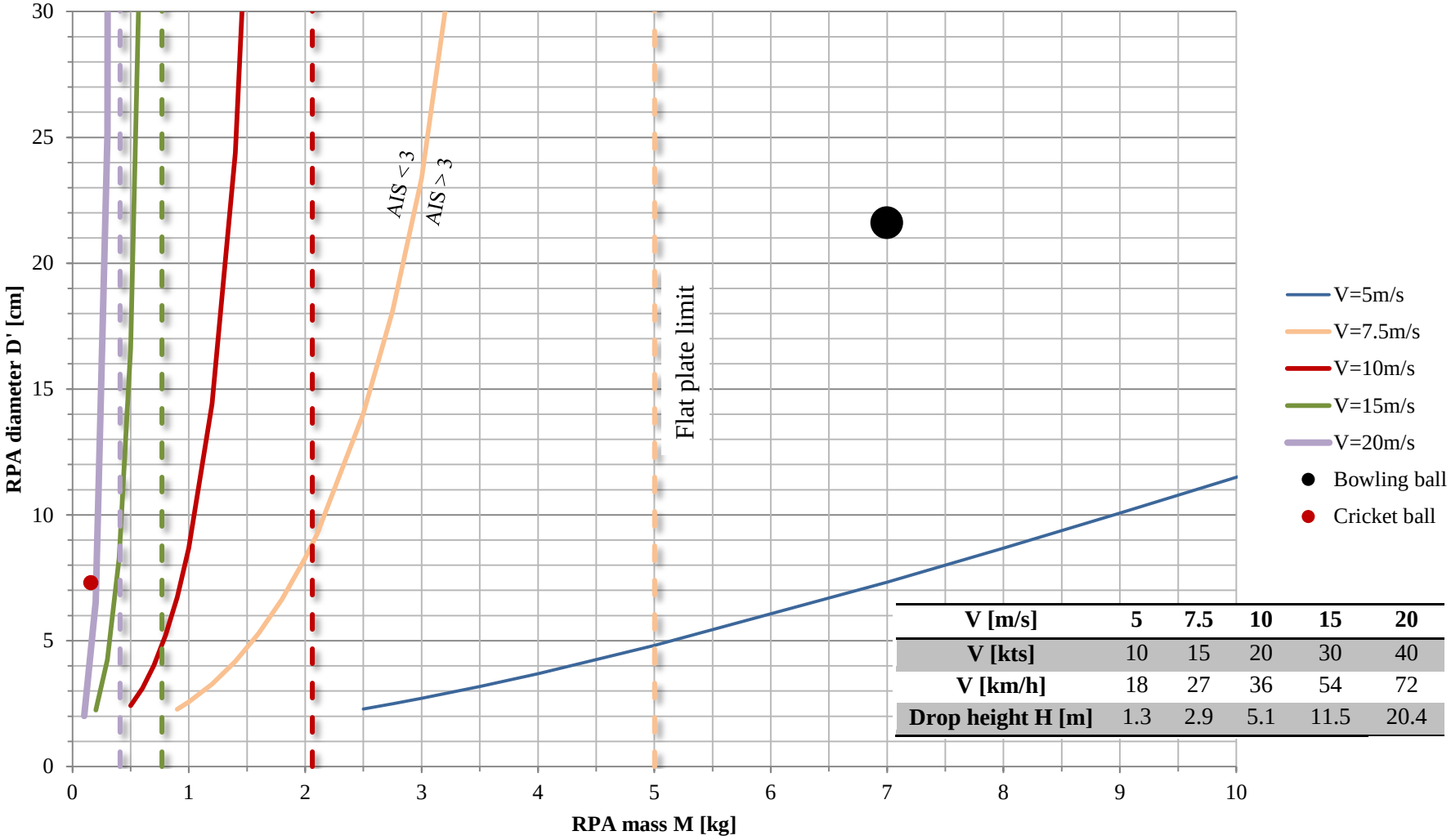

V [m/s]	5	7.5	10	15	20
V [kts]	10	15	20	30	40
V [km/h]	18	27	36	54	72
Drop height H [m]	1.3	2.9	5.1	11.5	20.4

Figure 12: 50% probability of skull fracture as a function of RPA impact velocity *V*, mass *M* and diameter *D'*.

8 Discussion of the model

As shown in Figure 13, the proposed injury model has three independent parameters: RPA velocity V and mass M, which contribute to the kinetic energy of impact, and the contact diameter D. The Blunt Criterion requires considering the characteristic diameter of the impacting RPA (or RPA part). This confirms the intuitive assumption that distributing the impact energy over a larger contact area reduces the injury potential. This approach is more reliable for chest injuries and less reliable for head injuries due to the more complex geometry and higher bone stiffness in the latter case. In any case, error bars of up to ±50% should be applied to the results.

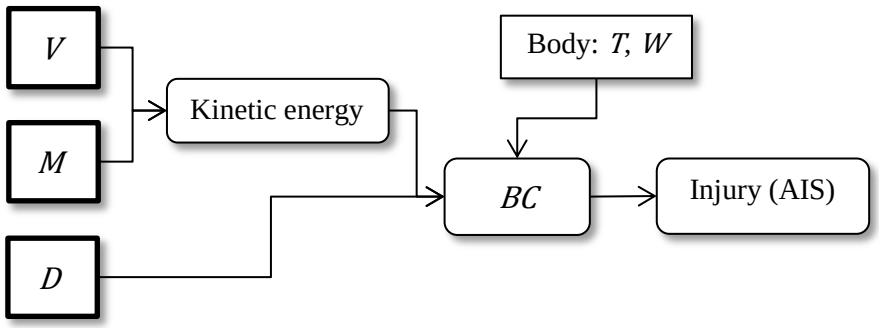

Figure 13: Independent parameters in the proposed model: velocity *V*, mass *M* and diameter *D*.

The model is likely to over-predict the thorax injury severity because the experimental data was obtained from cadaver experiments. (Sturdivan, et al., 2004) observed that dead soft tissue offers less resistance to impact, leading to apparent more severe injuries compared to live specimen.

The skull strength is determined by the thickness of the bone and overlaying soft tissue, which vary across the head surface. The model is based on experiments on the especially vulnerable temporo-parietal region; this is likely to over-predict the injury severity for head impacts.

The modelled victim is from the 5th percentile female population, which biological properties (50kg body mass, thin body wall) make this group most vulnerable. A 75kg male can tolerate more severe chest impacts; but weight and gender were found to not have a significant influence on the head injury tolerance.

The model has the following limitations:

1. The collision dynamics are ignored. The worst case scenario is assumed, in which the RPA impacts with its centre of mass. Any deviation from this scenario leads to lower impact energies.
2. The RPA material stiffness and frangibility are ignored. The current assumption of a rigid body predicts the highest possible deformation energies. Elastic deformations of the contacting RPA surface and/or the destruction of the hull components reduce the blunt injury severity by absorbing a large fraction of the kinetic energy. On the other hand, the creation of hull fragments increases the danger of lacerations and skin penetrating injuries. The regulatory requirement of energy absorbing materials is one possibility to reduce the injury potential.
3. Evidence suggests that chest impacts can be fatal even without leading to substantial physical damage, such as rib fractures (Maron, et al., 1995). Mainly small, fast moving objects (such

as baseballs) can interfere with the natural heart rhythm and lead to cardiac arrests in rare cases. Between 1977 and 1995, 25 fatal baseball chest impacts to youths were recorded in the US (Maron, et al., 1995). This type of injury is not captured by the present model.

4. Secondary injuries to the head and neck from high accelerations (brain concussions, Whiplash) are not captured by the present model. The kinetic energy not used for tissue deformation acts to accelerate the impacted body part (see Figure 2). For example, a 6kg RPA would transfer only 50 per cent of its kinetic energy as deformation energy to the head. The remaining energy would accelerate the head to 50 per cent of the RPA's impact velocity. Assuming an impact duration of 5ms and an impact velocity of V=15m/s, this results in an average acceleration of 150G. Under the rigid body assumption, skull fracture is predicted by the current model; yet padding the RPA with energy absorbing materials would increase the chance of high acceleration injuries.
5. The model assumes the free movement of the struck body part. If the movement is restricted, e.g. when hitting the head vertically from above or hitting a lying person, all kinetic energy is transformed into deformation energy. For RPA's lighter than 3kg, this can increase the inflicted energy by up to 30 per cent.
6. Finally, and most importantly, the model is an extrapolation of the Blunt Criterion, which is based on small projectiles (diameter of 2–4cm) and small mass (50–150g) impacting at high velocities (>20m/s). The short impact durations of such low momentum impacts lead to a high energy transfer rate from the projectile to the body, which might result in a different biomechanical response of the body compared to slower but larger impactors (Widder, et al., 1997). No experimental data using the blunt criterion with large impactors were found for an independent validation.

9 Conclusions

9.1 Summary

1. This study uses AIS=3 as the highest acceptable injury severity, which includes rib fractures or broken sternum for chest impact, and skull fracture for head impacts. The probability of death for this type of injury is less than 10 per cent.
2. The three parameters determining the injury severity are the RPA mass and velocity at impact, and the local radius (diameter) of the RPA part contacting the body.
3. For large impactor diameters (>30cm), the maximum tolerable deformation energies are 120J for the thorax and 76J for the head. The head impact scenario is the limiting case which prescribes the highest acceptable RPA velocity and mass.
4. For a 2kg RPA, the highest tolerable velocity for the head impact is below 7.5m/s (15kts). A minimum RPA part diameter of 10cm is required for this case. The impact energy is equivalent to a solid 11cm aluminium sphere dropped from a height of 3m.
5. A 2kg RPA at 10m/s is predicted to cause skull fracture, even when impacting with its flat side (equivalent to a 2kg aluminium plate dropped from a height of 5m).
6. The results are rough guides only, as the model's input variables show natural variation (e.g. biological parameters) or have been derived from a limited number of experiments. Error bars of ±50% should be applied.
7. The velocities in the loss-of-control scenario, in which the RPA descends from altitudes >60m reaching its terminal velocity, lie far above the determined acceptable values (typically above 30m/s). At such high impact velocities practically any RPA mass is likely to cause unacceptably severe injuries.

9.2 Recommendations

1. The exteriors of small RPA should be designed with as large as possible curvatures (local radius/diameter), within the practical limits of airframe size and aerodynamic considerations.
2. Sharp protrusions should be avoided, particularly beyond the foremost point of the airframe, to prevent skin-penetrating injuries.
3. The use of propeller fairings is recommended. Preference should be given to push propellers.
4. A designed frangibility of the RPA's airframe is recommended to reduce impact loads. Examples are designed weak points, e.g. in the arms of quad copters, or crumple zones on larger RPAs. Crashworthiness research from the automotive industry can provide design guidelines.
5. The following RPA mass and velocities should be regarded as limiting cases that prevent severe injuries:
    a. **0.4kg at 15m/s (30kts)**
    b. **1kg at 10m/s (20kts)**
    c. **2kg at 7.5m/s (15kts)**
6. These limits can be increased significantly by the use of energy absorbing materials for the RPA exterior. Deformable plastics or high density foam reduce the peak forces during impact (think of a soccer ball compared to a hollow aluminium sphere of the same mass & impact velocity).
7. Mitigation measures reducing the impact energy—such as automatically deployed parachutes or automatic descend at minimum velocity—should be employed in a loss-of-control situation.

10 APPENDIX

A. Calculation of the impactor diameter for head impact

Given the depth of the imprint deformation x_{def} into a soft sphere of diameter D_H and the effective diameter D, the associated impactor diameter D' can be calculated from the intersection of two circles. The relationship between D and D' is given by

$$D = \frac{1}{C}\sqrt{\left(-C+\frac{D'}{2}-\frac{D_H}{2}\right)\left(-C-\frac{D'}{2}-\frac{D_H}{2}\right)\left(-C+\frac{D'}{2}+\frac{D_H}{2}\right)\left(C+\frac{D'}{2}+\frac{D_H}{2}\right)}, \quad 15$$

where $C = \frac{D'}{2}+\frac{D_H}{2}-x_{def}$ is the distance between the sphere centres. This Equation is too complex to analytically determine D', and an approximation will be used based on a three-point arc radius as shown in Figure 14. The three points defining the arc are marked by crosses. The middle point is fixed at the distance x_{def} from the larger sphere's surface, while the outer two points slide along the red lines with the Equation: $h(D) = \frac{-x_{def}}{D_{FP}-2T_H}(D-2T_H)+x_{def}$. The radius of a three-point arc is:

$$r = \frac{D^2}{8h}+\frac{h}{2} \quad 16$$

Using $h(D)$ in Equation 16 and setting $D'=2r$, the diameter of the impactor becomes:

$$D' = \frac{D^2}{4x_{def}\left(1-\frac{D-2T_H}{D_{FP}-2T_H}\right)}+x_{def}\left(1-\frac{D-2T_H}{D_{FP}-2T_H}\right) \quad 17$$

The approximation over-predicts D' by up to 20 per cent for D'<20cm, which makes it conservative.

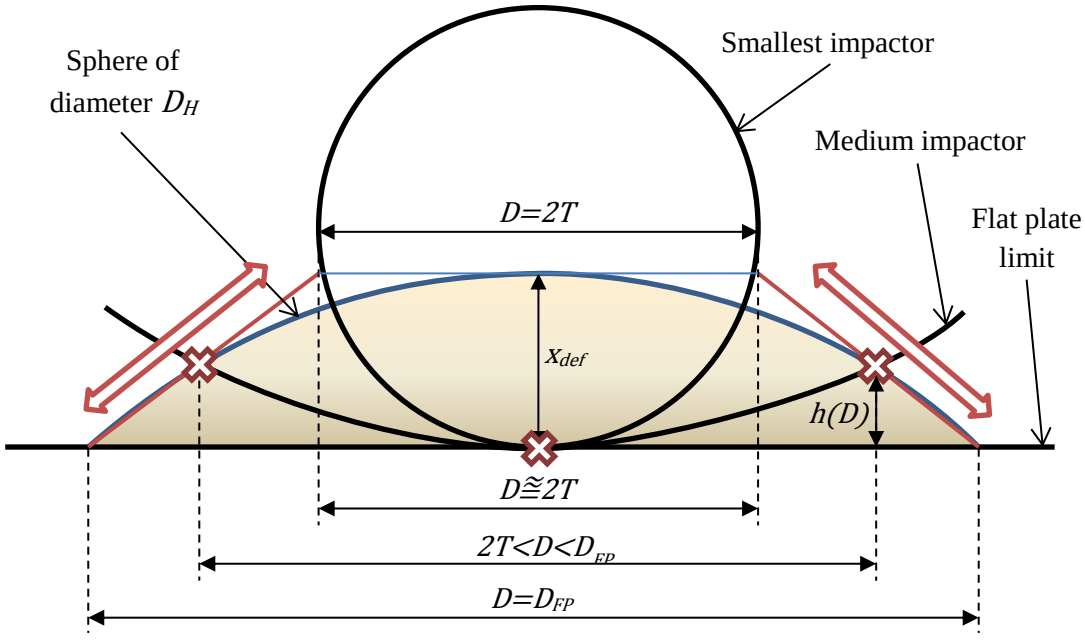

Figure 14:Geometry for calculation of the impactor diameter D' from a given effective diameter D.

B. Cutting injuries by rotating blades

Besides blunt trauma from an RPA impact, the possibility of a cutting injury from the rotating blades needs to be considered. This can be a spinning propeller of a fixed-wing aircraft or the rotating blades of a helicopter-type machine (most commonly a quad copter).

Limited literature could be found only for eye injuries: For blunt impacts by small projectiles (6mm in diameter), (Duma, 2005) compiled experimental data to derive a 50% probability for various eye injury severities. The impact energy thresholds are shown in Table 6.

Injury	Kinetic energy for 50% probability
Corneal abrasion	0.184J
Retinal damage	1.09 J
Globe rupture	4J

Table 6: Energy thresholds for blunt impact to the eye

(Alphonse, 2012) performed the only experiments found, in which actual RC (Remotely Controlled) helicopter blades were used on human cadaver eyes. The highest damage severity observed was corneal abrasion. Yet, the experiments are not well documented, and the helicopters used are very light indoor models, with weak motors and light blades. Actual quad-copters in the 1–4lb range should be expected to have a higher damage potential.

C. 7kg limit justification

It is desirable to define a second – larger – weight limit for large RPA, above the 2kg cut-off. The proposed model does not provide a criterion which would justify any specific weight limit. In particular, an impact with any weight above 2–5kg by far exceeds the defined injury criterion, and is most likely to lead to life threatening injuries.

It is recommended to use a kinetic energy limit, as proposed by (Clothier, et al., 2010). Accepting the fact that high kinetic energy values (>200–500J) are likely to lead to a fatality upon impact, the focus should be shifted from human injury to damage to structures. It is suggested to use penetration of houses by the impacting RPA as damage criterion. This scenario includes (most likely fatal) injuries to people inside the shelter, who are endangered by the remaining kinetic energy of the RPA and debris after structure penetration. The non-penetration of a representative shelter by an impacting RPA is a viable criterion.

The properties of a 'representative shelter' depend on the building material, particularly the roof. (Clothier, et al., 2010) state approximately **1400J** as the lower limit for the penetration of a residential home with a corrugated-iron roof. Using this value, the following mass limits are proposed:

a) 12kg @ 15m/s (30kts)
b) 7kg @ 20m/s (40kts)
c) 3kg @ 30m/s (60kts)

11 Bibliography

321-00, S. t. s. R., 2000. *Common Risk Criteria for National Test Ranges,* US Army White Sands Missile Range, New Mexico: Secretariat, Range Commanders Council.

Alphonse, V., 2012. *Injury Biomechanics of the Human Eye,* s.l.: Virginia Polytechnic Institute and State University.

Clare, V., J., L., A., M. & Sturdivan, L., 1975. *Blunt trauma data correlation,* s.l.: Edgewood arsenal Aberdeen proving ground.

Clothier, R., Palmer, J., Walker, R. & Fulton, N., 2010. *Definition of airworthiness categories for civil Unmanned Aircraft Systems (UAS).*. Acropolis Conference Centre, Nice, s.n.

Duma, S., 2005. Determination of Significant Parameters for Eye Injury Risk from Projectiles. *The Journal of TRAUMA, Injury, Infection, and Critical Care,* Volume 59, pp. 960-964.

Frank, M., 2012. When backyard fun turns to trauma: risk assessment of blunt ballistic impact trauma due to potato cannons. *International journal of legal medicine,* 126(1), pp. 13-18.

Haddon, D. & Whittaker, C., 2004. *UK-CAA policy for light UAV systems,* s.l.: UK Civil Aviation Authority.

Hamel, A. et al., 2013. Effects of fall conditions and biological variability on the mechanism of skull fractures caused by falls. *International journal of legal medicine,* 127(1), pp. 111-118.

Lim, D., 2005. *Free vibration response of the human head and neck system under normal and mouthguard conditions.* s.l.:Simon Fraser University, Canada.

Magister, T., 2010. The small unmanned aircraft blunt criterion based injury potential estimation. *Safety Science,* Volume 48, p. 1313–1320.

Maron, B., Poliac, L., Kaplan, J. & Mueller, F., 1995. Blunt impact to the chest leading to sudden death from cardiac arrest during sports activities. *New England Journal of Medicine,* 333(6), pp. 337-342.

Raymond, D., Van Ee, C. & Bir, C., 2009. Tolerance of the skull to blunt ballistic temporo-parietal impact. *Journal of Biomechanics,* Volume 42, pp. 2479-2485.

Raymond, D. E., 2008. *Biomechanics of blunt ballistic temporo-parietal head impact.* Wayne State University, Detroit, Michigan: s.n.

Sturdivan, L., Viano, D. & Champion, R., 2004. Analysis of injury criteria to assess chest and abdominal injury risks in blunt and ballistic impacts. *The Journal of TRAUMA, Injury, Infection, and Critical Care,* 56(3), pp. 651-663.

Thollon, L., Llari, M., André, L. & Pascal Adalian, G., 2013. Biomechanical analysis of skull fractures after uncontrolled hanging release. *Forensic Science International,* 233(1), pp. 220-229.

Viano, D., Andrzejak, D., Polley, T. & King, A., 1992. Mechanism of fatal chest injury by baseball impact: development of an experimental model. *Clinical Journal of Sport Medicine,* 2(3), pp. 166-171.

Widder, J., Butz, D. & Milosh, J., 1997. *Assessing the Blunt Trauma Potential of Free Flying Projectiles for Development and Safety Certification of Non-Lethal Kinetic Energy Impactors,* s.l.: Battelle Columbus Operations.

Yoganandan, N. & Pintar, F., 2004. Biomechanics of temporo-parietal skull fracture. *Clinical Biomechanics,* Volume 19, p. 225–239.

2013

Potential damage assessment of a mid-air collision with a small UAV

Civil Aviation Safety Authority

Civil Aviation Safety Authority / Monash University

12/6/2013

Revisions

Date	Name	Notes
06.12.2013	Alexander Radi	Initial version 1.0

Executive summary

This report analyses the damage potential to manned aircraft from a mid-air collision with a small unmanned aircraft (UAV). The scenarios of engine ingestion and impacts into fuselage and cockpit windscreen are considered. The aim of the study is to provide velocity estimates, above which penetration of the aircraft structure can be expected. The consequences of the penetration will depend on the impact location, and are not explored in this report.

The method is a combination of reviewing published experimental data and performing original computations using a semi-empirical model. The literature research concentrates on the fields of range safety (RCC, 2007) and uncontained engine failure tests, all of which deal with the penetration of aircraft aluminium plates by compact, fast moving metal fragments. Bird impact studies into windscreens and fuselage were reviewed, but were found of limited value due to the different impact behaviour of organic material compared to components constituting a typical UAV. Assuming that the highest threat of penetration is from the most compact and heavy components of an UAV, a detailed damage analysis of single component impacts (battery pack, motor, payload) was performed using computer simulations (Monte Carlo method).

Literature suggests that ingestion into one engine, and the subsequent thrust loss, is the most likely collision scenario (3 out of 4 cases); the consequences are not likely to be catastrophic, as modern jet aircraft are designed to continue safe flight with one engine loss. For collision velocities above 200kts, UAV parts are predicted to penetrate the fuselage skin, with the potential of damaging internal systems. At landing velocities of large commercial aircraft (V_{FE}=160—180kts), penetration of the cockpit windscreen is not likely to occur for small UAVs below 2kg; penetration should be assumed for heavier UAVs. General aviation windscreens will be penetrated at typical cruise velocities, regardless of UAV size/weight.

The equation used for penetration prediction was originally developed for metal plates. Its application to windscreens bears large uncertainties. As no experimental data exist to validate the predictions for windscreen materials, the results should be regarded as rough estimates. It is recommended to commission impact tests of solid objects into windscreen samples.

Abbreviations

Abbreviation	Definition
2D	Two-dimensional
3D	Three-dimensional
CASA	Civil Aviation Safety Authority
CASR	Civil Aviation Safety Regulations
CFR	Code of Federal Regulations
CS	Certification Specifications
FAA	Federal Aviation Administration
FAR	Federal Aviation Regulations
ft/s	Feet per second
GA	General Aviation
kts	Knots
MPa	Mega-Pascal (10^6 N/m^2)
MTOW	Maximum Takeoff Weight
RMIT	Royal Melbourne Institute of Technology
UAS	Unmanned Aerial System
UAV	Unmanned Aerial Vehicle
V_{50}	Ballistic limit velocity
V_C	Cruise velocity
V_{FE}	Maximum flap extended velocity

1 Table of Contents

2 Introduction

2.1 Objectives

This report presents the findings of a study carried out by Alexander Radi M.Sc.[1] during a 4 months research internship at CASA (Canberra). The aim of the study is to provide the Standards Development branch at CASA with a potential damage assessment of a mid-air collision between a manned aircraft and a small UAV (MTOW<5kg). The focus is on multi-rotor UAVs ('quad-copters') due their wide spread and availability. The impact into the jet engines, windscreen and fuselage are considered. The work aims to derive critical collision velocities above which UAV components are likely to penetrate into the aircraft interior. The consequences of such penetration are briefly discussed, but their detailed analysis is outside the scope of this report.

2.2 Background

Unmanned Aircraft Systems (UAS) is the fastest growing sector of the aviation industry today, with sales expected to top $15 billion by 2014 (RMIT[2]). Nevertheless, a broad range of safety, regulatory, social and technical challenges need to be addressed before the sight of an unmanned aircraft in the sky becomes as common and accepted by the public as its manned counterpart.

Separation, and ultimately collision avoidance ("sense and avoid"), is one of the major technological challenges currently preventing the implementation of the UAS into the controlled airspace. The possibility of a mid-air collision between a conventional aircraft and an UAV is present already today, as limited UAS operations are permitted even without the existence of an effective sense and avoid technology[3]. The consequences of such collisions are not necessarily catastrophic due to the usually low UAV mass, but need to be better understood to assess the overall risk posed by the future increased UAV traffic.

2.2.1 Aircraft impact location

The consequences of a mid-air collision with an UAV will strongly depend on the aircraft impact location. Statistics on bird strikes can be used to assess the likelihood of an aircraft part being struck. Figure 1 shows that engine ingestion occurred in 76% of all recorded bird strikes involving transport category aeroplanes, followed by impacts into the windshield with 7%. In general aviation (GA), the windshield is struck in 56% of all cases, followed by the engine.

[1] Ph.D. candidate Aerospace Engineering at Monash University, Melbourne
[2] http://www.rmit.edu.au/research/institutes/platformtechnologies/uav
[3] CASR 1998, Part 101F

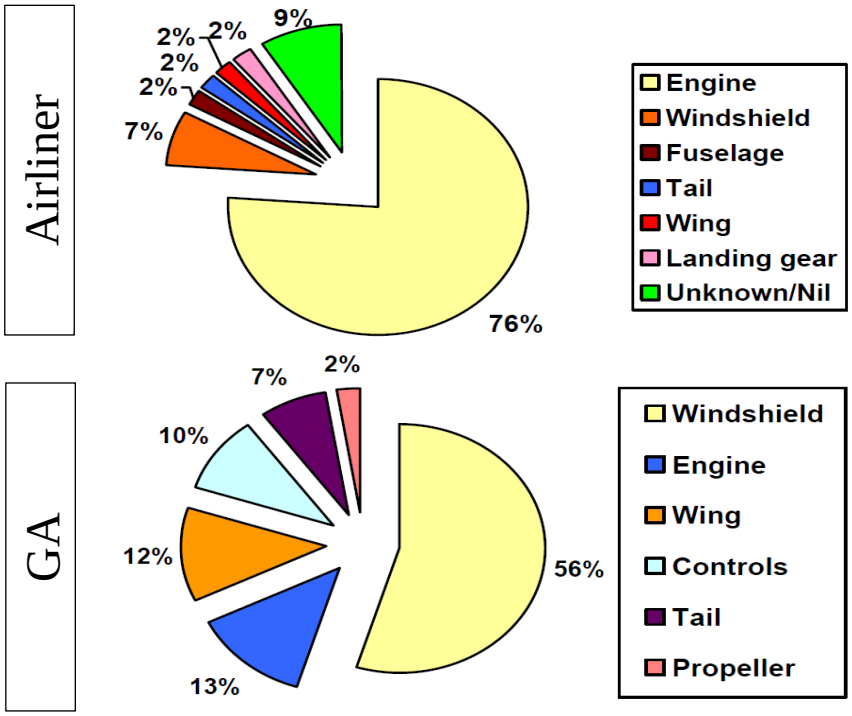

Figure 1: Location of bird strikes for commercial airliners (top) and general aviation (bottom) worldwide for 1912-2011 (Thorpe, 2012).

These data imply that the UAV is most likely to be ingested into one of the jet engines on a commercial airliner, rather than hitting any other aircraft part. The consequences of an engine impact will be discussed in 3. The windscreen penetration is studied in 4.5.

For GA (both fixed and rotary wing), the consequences of a collision are more severe, as the windshield is the most likely part to be struck, and which leads to a fatal outcome in the most cases (Figure 2). The windscreens in this aircraft category are usually made of thin acrylic, and are not required to be able to withstand any bird impact[4]. This lack of design requirements puts the pilot and passengers at high risk, as already a 40g bird can penetrate the windscreen (Thorpe, 2012). In addition, avoidance manoeuvres of general aviation pilots have led to fatal crashes in the past, something that is a possibility during an encounter with an airborne UAV. Section 4.5.3 shows that for GA category, penetration of the windscreen is predicted in all cases at cruise velocity.

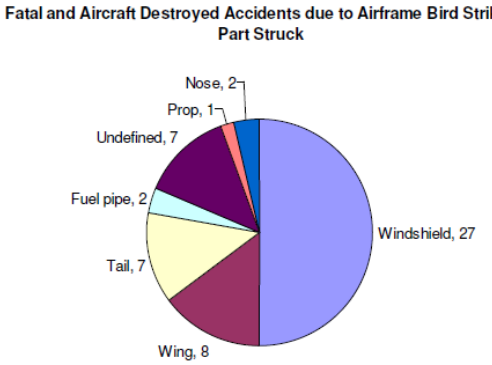

Figure 2: Parts struck during non-engine bird strike accidents (GA aircraft) (ATKINS, 2008).

[4] Under FAR-23 and CS-23, only the windscreens of the commuter category are required to withstand an impact of a 2lb bird at maximum approach flap speed [FAR § 23.775(h)(1)].

3 Engine ingestion

As discussed in the previous section, engine ingestion is the most often reported type of bird strike for commercial airliners (76%), followed by windscreen damage. The predominance of engine impacts is rather surprising, as the engine capture area (cross-sectional area of the airstream into all engines) is only 2—4% of the overall frontal area of a turbofan aircraft (Cole, et al., 1997). Nevertheless, the same probability will be assumed for the UAV impact, which means that 3 out of 4 occurrences should result in ingestion of the UAV.

The consequences of the ingestion depend on whether the foreign object enters the engine core or by-passes it. Only a part of the air processed through a turbofan engine actually goes through the engine core, which contains the compressors, burners and turbines. The rest passes only through the fan; the bypass ratio of modern engines can exceed 8. In general, the greater the bypass ratio is, the smaller the chance that an object will enter the engine core (Cole, et al., 1997).

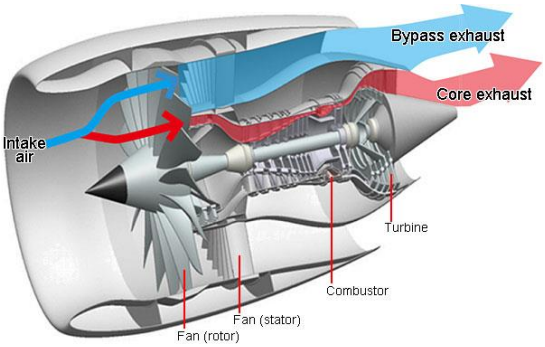

Figure 3: Modern turbofan engine with a high bypass ratio.

In any case, substantial damage to the fan blades should be expected. Even the ingestion of a bird, which behaves like a fluid at high impact velocities, results in large blade deformations (Figure 4). Although certification standards require the engines to tolerate the impact by birds of a certain size[5], and the involved impact physics are being studied in detail (Vignjevic, et al., 2013), no experimental studies could be found on the consequences of the ingestion of solid objects.

This CRJ600 with 20 passengers on board ingested doves into #1 engine at rotation from a southern USA airport. The engine sustained substantial damage and the aircraft was forced to make a precautionary landing.

Figure 4: Fan blade damage from bird strike (Cleary, et al., 2006).

[5] EASA Airworthiness Code CS-E 800 'Bird Strike and Ingestion'; corresponding FAA requirements are given in CFR Part 33

The most likely consequence of solid object ingestion is the partial or total loss of engine thrust. This can be expected for metal objects as light as 1g entering the engine core (Cole, et al., 1997) (RCC, 2007). This foreign object ingestion can be accompanied by the throw of fan blade fragments or compressor blades, with subsequent penetration of other aircraft parts.

The danger to the aircraft from such events is solely based on past experiences of uncontained engine failure and expert opinions. (Wilde, 2010) quotes FAA experts and guidelines, stating "that debris ingestions into commercial aircraft engines are unlikely to generate a potentially catastrophic condition due to engine fragment throw. Specifically, the experts reported that (1) engine ingestion of a fragment less than 300 grams is unlikely to produce uncontained impacts other than perhaps some fan blade fragments, (2) experience shows that uncontained fan blade impacts have the potential to impact the fuselage, causing injury, significant damage to the plane, or decompression, but (3) this is less than a 1 in 100 occurrence".

It can be assumed that the loss of one engine will not result in a catastrophic failure. Current law for commercial transport aircraft requires designs that enable continued safe operation following any single engine loss (14 CFR §25.903(b)). Empirical data indicates about one out of a thousand engine losses results in a catastrophic outcome (Wilde, 2010).

The conclusion for the present study is that an ingestion of the UAV into one of the engines is the most likely event, but which is unlikely to result in in a catastrophic outcome.

4 Impact damage

Besides ingestion into the engine, the collision of the UAV with the remaining frontal area of an aircraft can result in parts of the UAV penetrating into the interior of the aircraft structure. The consequences of penetration will depend on the impact location, and can include, but are not limited to: damage of electrical or hydraulical systems or other control systems, penetration of the fuel tank, weakening of the structural elements (stringers, spars) or injury/fatality of crew members or passengers.

4.1 Bird impacts

One way to assess the damage potential of UAV impacts into the fuselage and windscreen is to analyse past occurrences and studies of bird impacts. Bird impacts into the fuselage can result in substantial local damage (Figure 5), and can potentially lead to catastrophic consequences if the windscreen is penetrated. Fuselage collisions with birds up to 4lb mass are covered by FAR-25, which requires the "continued safe flight and landing after impact with a 4lb bird at cruise speed (V_C) at sea level or $0.85V_C$ at 8000ft (2438 m), whichever is the most critical". The same requirement applies to windshields and supporting structure, which "are to withstand the above impact without penetration or critical fragmentation".

Figure 5: Damage to a Boeing 747 flap after a bird collision at 1200 feet AGL (Cleary, et al., 2006).

It appears questionable that the collision with a rigid UAV is comparable to the impact of a 'soft' bird. Birds, and organic materials in general, behave like fluids during a high-speed impact. Figure 6 shows the flowing behaviour of a simulated bird during an impact into a flap section at 194kts. The disintegration and the flowing of the bird absorb energy, which decreases the impact forces. A non-deformable impactor, such as an UAV component, creates a localized strain field in the target material with high peak forces, which supports a 'plugging' as material failure mode. The high peak forces are likely to result in penetration at lower impactor masses compared to birds. This report will assume non-deformable impactors with a plugging penetration mode.

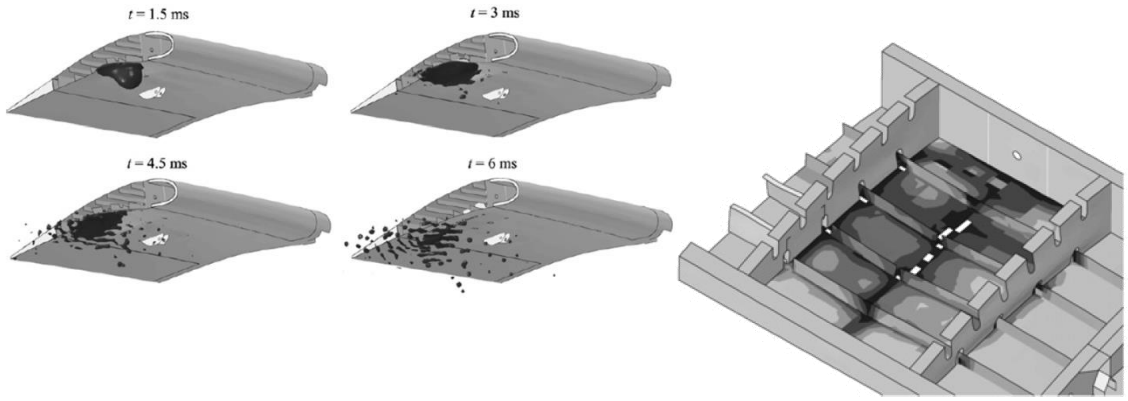

Figure 6: Impact of a 4lb bird into an extended flap at 100m/s (194kts) (Smojver & Ivancevic, 2011).

4.2 Breakdown of a typical UAV structure

This chapter will estimate the impact velocity above which penetration of the aircraft's metal skin can be expected (*ballistic limit*). Due to the complexity of the typical UAV airframe, only the impact of selected UAV components will be modelled.

Currently, the most common UAV type on the market, and which is easily custom made by hobbyist, is the quad copter type UAV (Figure 7). Its airframe consists of an even number of arms holding electrical motors at their ends. The controller, battery and payload are positioned at the hub of the arms. The collision behaviour is complex and depends on the strength, frangibility, relative orientation and mass of the structural elements. A simple analytical model of the whole system is impracticable, and no experimental results exist to create an empirical model. Due to the exposed location of the single components (motors, battery pack), it is suggested to study only the collision of the most dense and heavy parts. The frame holding these parts is assumed to provide no significant resistance upon impact. This is justified, as frames are often made of aluminium tubes, carbon fibre or plastic plates, or balsa wood. This approach simplifies the analysis by allowing the modelling of the separate components as simple geometric objects, such as cylinders or blocks (see Appendix B for details).

A 'small' and a 'big' quad copter will be used as a case study, representing an UAV with a mass of less than 2kg and 2—5kg, respectively. The densest and heaviest parts, which pose the biggest risk of penetration upon impact, are the motors, battery pack(s) and the camera as a typical payload. Figure 7 shows two typical UAVs and their components. Components that will be modelled in the present study were selected from an online hobby store. Table 1 lists the dimensions and weights. These parts are representative only, and do not necessarily comprise a realistic UAV configuration.

The largest motor in Table 1 ('motor C'), combined with 'battery B' of the big quad-copter, represent a fixed-wing UAV. Due to its size and weight, this motor can be used interchangeably with a combustion engine in fixed-wing UAVs (the manufacturer advertises it as a replacement for a 100cc piston engine).

One limitation of the present approach is the assumed infrangibility of the components, which behave like solid blocks of metal upon impact (the density of the parts is similar to aluminium). The results of the calculation should be regarded as conservative, as the parts would experience strong deformations, and might disintegrate completely upon impact. Particularly, the battery pack consists of single cells held together by tape, which makes it quite flexible. Yet, the close proximity of these cells upon impact, and the resulting combined loads, justify modelling the battery pack as a solid block.

Figure 7: Typical quad copter UAV configurations. Top left: small machine; top right: big machine; bottom: typical structural elements and payloads.

	Item	Model	Geometry	Dimensions [mm]	Weight [g]
Quad-copter (small)	Motor A	NX-4006-530kv	Cylinder	D=45, L=12	67
	Battery A	--	Block	25x50x65	160
	Camera A	GoPro Hero 2	Block	42x60x30	190
Quad-copter (big)	Motor B	Turnigy Multistar 4830-480Kv	Cylinder	D=47, L=33	154
	Battery B	--	Block	45x45x138	583
	Camera B	Canon EOS 7D	Block	148x110x74	820
Single-engine	Motor C	Turnigy CA120-70 (100cc eq)	Cylinder	D=118, L=120	2730

Table 1: Dimensions and weights of representative UAV components.

4.3 Modelling the penetration of plates

4.3.1 The ballistic limit

Whether a compact impactor penetrates a flat plate, depends on a series of physical and geometrical parameters, which will be introduced in 4.3.2. The relationship between these parameters has been studied extensively in three fields of application:

A. Ballistic weapon projectiles penetration into steel/armour plates (Goldsmith, 1999)
B. Aircraft collision with debris generated from orbital missile explosions (RCC, 2007)
C. Uncontained engine failure with debris penetration of the aircraft fuselage (Lundin, 2002)

Common to all three examples is the relatively high velocity range, with velocities over 1000ft/s (>590kts) in application A, 700-800ft/s (415—470kts) in B, and 300—800ft/s (177—470kts) in C. The present report will use methods and models from application C, which deals explicitly with aircraft materials (aviation-grade aluminium) and has experimental and numerical data at impact velocities as low as 150ft/s (90kts).

Beginning 2000, the FAA commissioned an extensive experimental study on the consequences of uncontained engine failure, the Uncontained Engine Debris Mitigation Program: UEDMP (Lundin, 2001) (Lundin, 2002). The study examined the impact of turbine engine blade fragments into the fuselage. Of interest for the present report is the estimation of the *ballistic limit* velocity V_{50}, which is classically defined as the velocity with a 50% probability of penetration.

Intuitively, the mass of the impacting object and the plate thickness will be among the variables determining the ballistic limit. Figure 8 shows experimental results of the impact of a 1/2" steel sphere into 1/16”, 1/8” and 1/4” thick aluminium plates. It can be seen that above a certain impact velocity the residual velocity of the impactor is larger than zero, meaning the impactor has penetrated the plate. The velocity, at which the data points raise for the first time above the horizontal, is the ballistic limit V_{50}. As expected, thicker plates require higher velocities for penetration. The higher the impact velocity of the impactor, the higher the residual velocity of the projectile exiting the rear side of the plate will be.

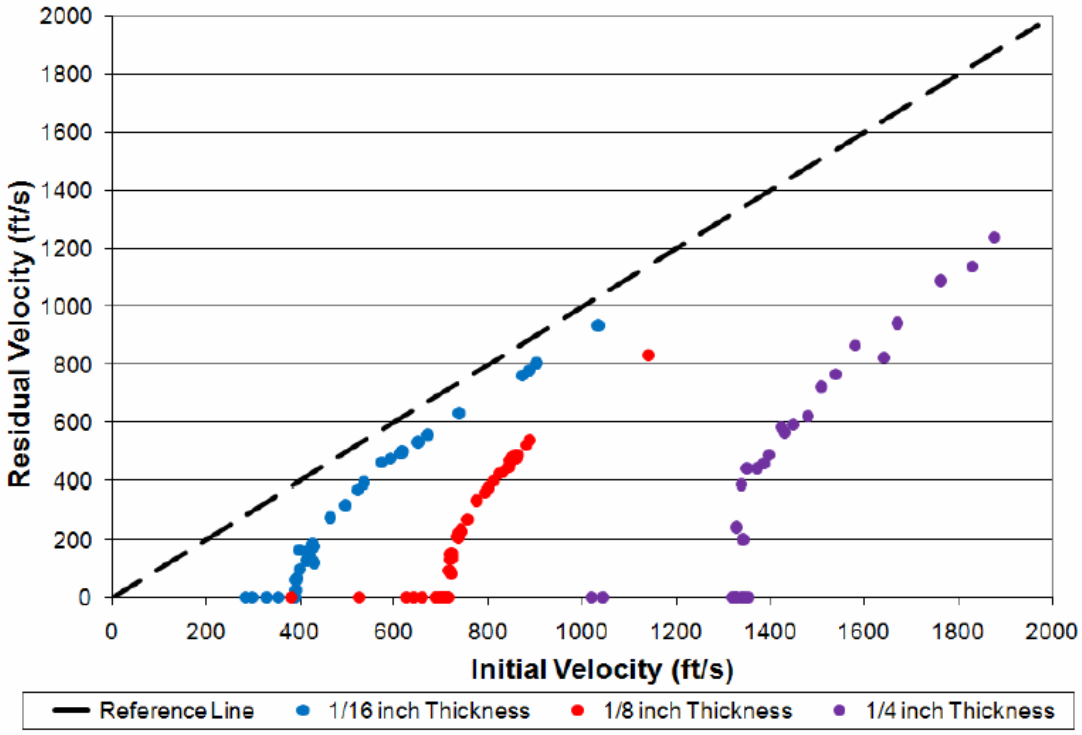

Figure 8: Experimental ballistic limit evaluation for aircraft aluminium plates at different target material thicknesses. The impactor is a 1/2” diameter steel sphere. From (Buyuk, et al., 2008).

4.3.2 The FAA penetration equation

The FAA penetration equation will be used for the prediction of the ballistic limit V_{50}. This equation is based on the energy required to punch a round hole in a sheet of metal. More details on the assumptions and limitations can be found in Appendix A. The equation is defined as:

$$V_{50} = \sqrt{\frac{2LC_S t^2}{m\cos^2\theta}}$$

where

- m = the mass of the projectile [kg]
- θ = the obliquity [radians]; see Figure 9
- C_S = an empirically determined shear constant [Pa], which is roughly correlated with classical material properties
- L = the perimeter of the subtended presented area of the projectile [m]: in the case of impacts with obliquity this is the area of the projectile normal to the velocity at impact and projected onto the target (e.g. roughly the perimeter of the hole in the target)
- t = the thickness of the target material [m].

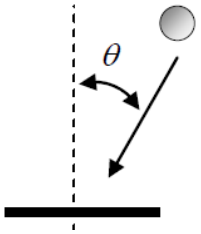

Figure 9: Geometry of the oblique impact.

V_{50} is classically defined as the velocity where there is a 50% probability of penetration. However, the FAA penetration equation is deterministic and intended to provide a conservative estimate such that no penetration is predicted for impacts at velocities less than V_{50}, and penetration is predicted for impact velocities greater than V_{50}.

A *boxplot* will be used in this report to depict the ballistic limit. This representation expresses the probabilistic nature of the impactor orientation relative to the impact plate. The impact area perimeter shows a certain probability distribution, from the least likely (usually the head-on impact with the smallest area) to the largest impact area. The calculation of the probabilities, and an explanation of the boxplot, can be found in Appendix A—C.

4.4 Impact: Fuselage and wings

The consequences of aircraft skin penetration by UAV parts will depend on the impact location, and can lead to damage of electrical or hydraulical systems or other control systems, penetration of the fuel tank, weakening of the structural elements (stringers, spars) or injury/fatality of crew members or passengers.

4.4.1 Penetration: Fuselage and wings

The fuselage skin is modelled as 1/8” and 1/16” thick aluminium plates (C_S=276MPa), under a perpendicular impact. To put the values of V_{50} in perspective, the maximum velocity with fully extended flaps of a Being 747-400 (V_{FE}=180kts) and a Boeing 737-400 (V_{FE}=162kts) are plotted for comparison. This is the highest expected velocity of a commercial airliner during landing.

Figure 10 shows the ballistic limits of a 1/8” aluminium plate for components of a small UAV, big UAV and a single engine fixed-wing UAV (compare Table 1). All components of the big UAV, and the battery and camera of the small UAV, are likely to penetrate the aircraft skin at velocities even below V_{FE}. The 2.73kg heavy motor of the fixed-wing UAV (motor C) causes a penetration already at 60kts.

Figure 11 shows the ballistic limits for an impact into a 1/16” skin section. All UAV components are likely to penetrate the skin for velocities above 100kts.

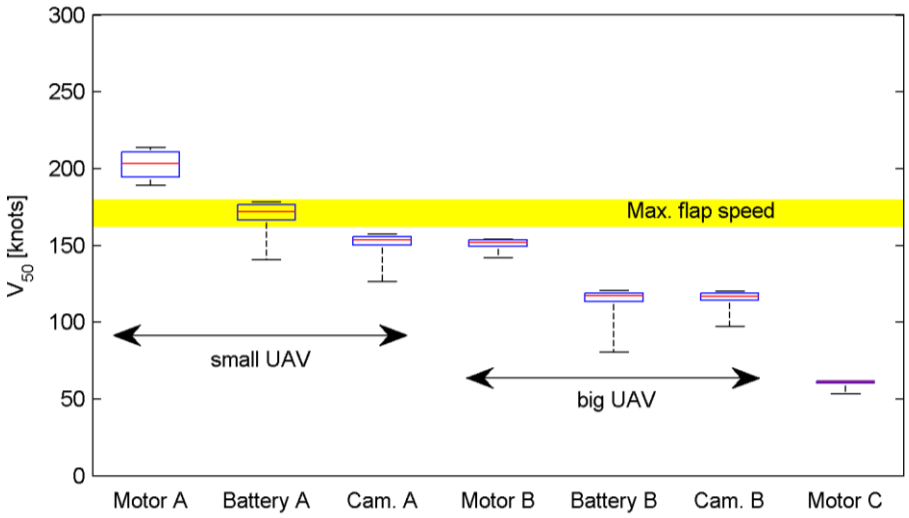

Figure 10: Ballistic limit of 1/8” thick aluminium skin (normal impact).

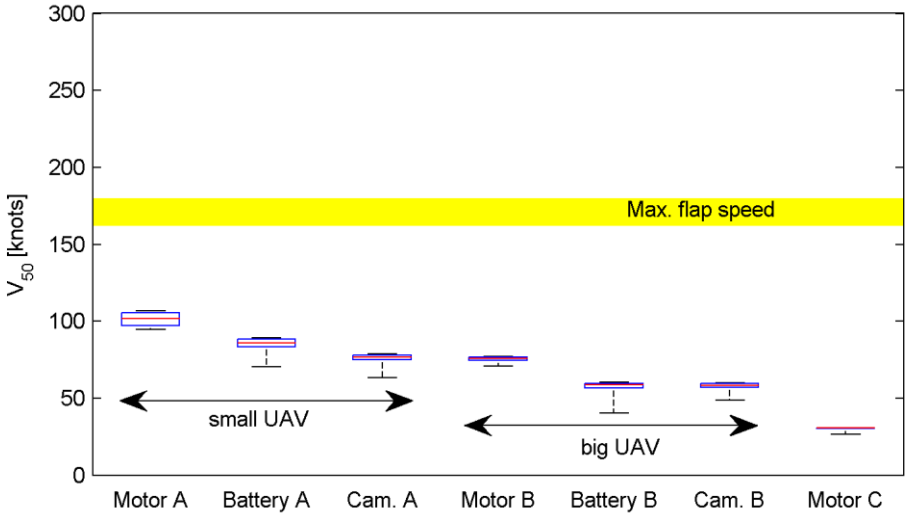

Figure 11: Ballistic limit of 1/16” thick aluminium skin (normal impact).

4.5 Impact: Windscreen

The impact into the windscreen adds two complications:

1. The windscreen is inclined with respect to the flight path.
2. The impact physics of the windscreen material differ from a metal.

4.5.1 Validity of the FAA penetration equation

The inclination of the windscreen is taken into account in the FAA equation by the oblique angle θ. There is evidence that the material response to an oblique impact does not follow a simple $\cos\theta$-law (Wilde, 2010), and the FAA equation should be modified to improve its prediction capability. Yet, the large uncertainties introduced by the consideration of a non-metal plate as a target outweigh any gains from the modified equation. The unmodified equation will be used in the present study for simplicity.

The use of a non-metal target material leads to large uncertainties in the results. The FAA equation was developed from and for impacts into metal plates. In particular, the possible change of the failure mechanism is a potential source of error. The empirical constant C_S incorporates the shear strength *and* the failure mechanism ('mode') that occurred during the experiments that the constant was derived from. Two common failure modes are 'petaling' and 'plugging' (Figure 12), in case of thin and thick metal plates, respectively (Buyuk, et al., 2008). When considering a non-metal windscreen, the material's impact resistance is accounted for by substituting C_S with the material's shear strength; yet, this does not take into account a possible change of failure mechanism. The present results for windscreen penetration should be treated as rough estimates with large error bars.

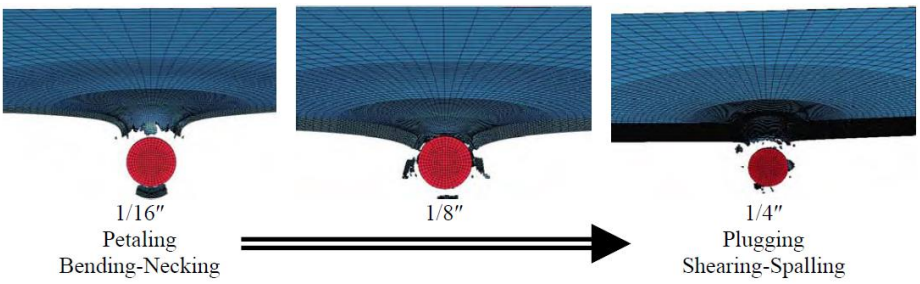

Figure 12: Transition of failure mode form 'petaling' to 'plugging' depending on plate thickness.

To make things more complex, the windscreen is usually a multilayer construction of glass and vinyl, resulting in a combination of brittle and elastic behaviour. No experimental data could be found on the impact behaviour (e.g. shear strength) of such composite materials. Some literature suggests modelling the windscreen as a 1/2" thick Lexan, cast acrylic, stretched acrylic, or bullet resistant glass plate (Cole, et al., 1997), while others assume the windscreen's ballistic resistance to be equivalent to a 1/8" thick aluminium plate (Wilde, 2010). Both options will be compared in the present study: a 1/2" thick Lexan plate and a 1/8" thick aluminium plate, both at 40° incidence. In addition, the windscreen of a GA aircraft will be modelled as a 1/8" thick Lexan plate (Table 2).

	Material	Shear strength (ultimate)	Thickness	Notes
#1	Aluminium	276 MPa	1/8"	(Wilde, 2010)
#2	Lexan	68 MPa[6]	1/2"	(Cole, et al., 1997)
#3	Lexan	68 MPa	1/8"	GA windscreen

Table 2: Material properties of the modelled windscreens.

4.5.2 Penetration: Airliner windscreen

Figure 13 shows the ballistic limits for a windscreen modelled as a 1/8" aluminium plate. Only components of the big UAV (and the exceptionally large fixed-wing motor C) are expected to penetrate the windscreen.

Interestingly, any penetration becomes unlikely when the windscreen is modelled as a 1/2" Lexan plate, as shown in Figure 14 (with the exception of motor C). The decreased strength of Lexan is more than balanced by the four-fold increase in plate thickness, compared to the aluminium model. This discrepancy makes the prediction of windscreen penetration ambiguous. It is recommended to accept the more conservative results of Figure 13.

[6] http://www.associatedplastics.com/forms/pc_lexan_9034.pdf

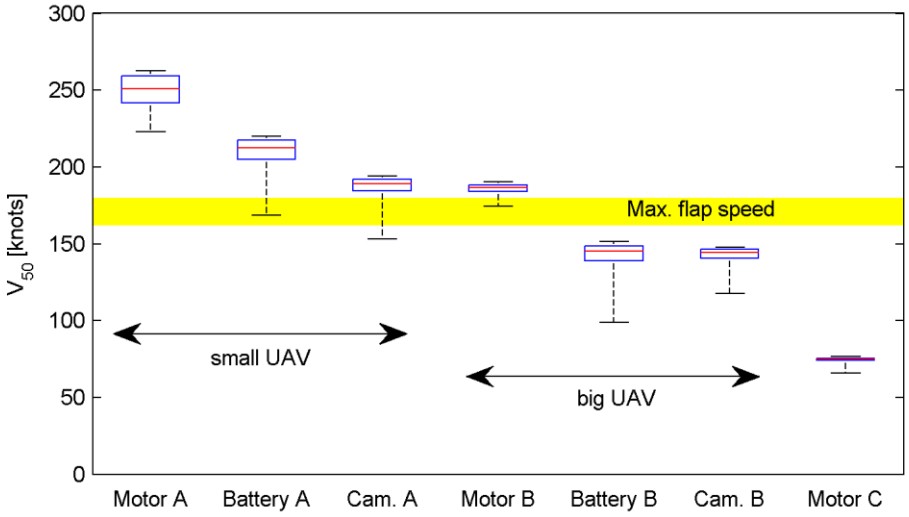

Figure 13: Ballistic limit of the airliner windscreen (40° inclination), modelled as a 1/8" aluminium plate.

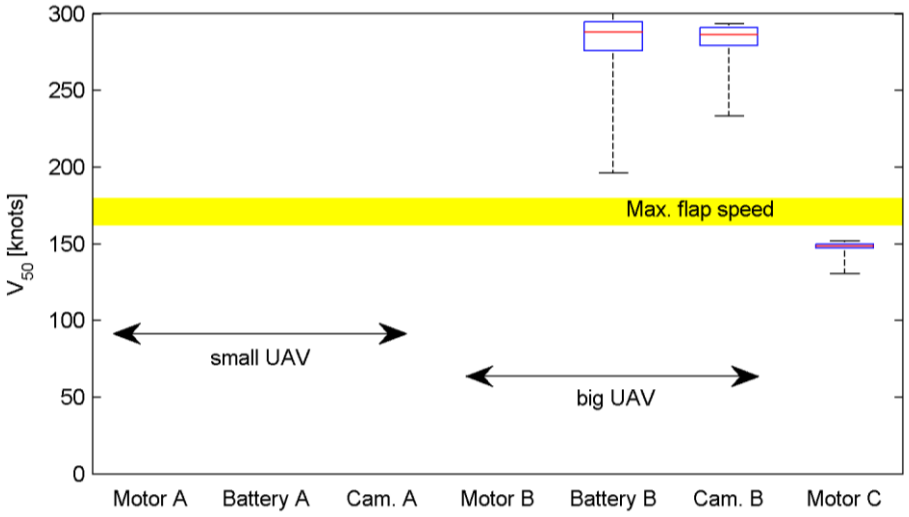

Figure 14: Ballistic limit of the airliner windscreen (40° inclination), modelled as a 1/2" Lexan plate.

4.5.3 Penetration: General aviation windscreen

The ballistic limits for the penetration of a GA windscreen (1/8" Lexan) are compared to the maximum cruise speed V_C (124kts), and maximum flaps extended speed V_{FE} (87kts) of a Cessna Skyhawk[7]. Figure 15 shows that windscreen penetration can be expected in all cases at cruise speed. In landing configuration (V_{FE}), only components of the big UAV (and motor C) are likely to penetrate the windscreen.

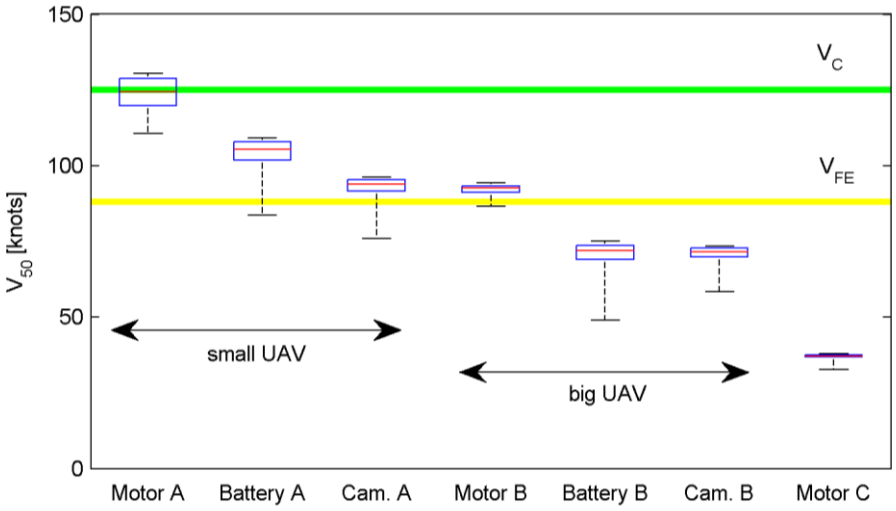

Figure 15: Ballistic limit of a GA windscreen, modelled as a 1/8" Lexan plate (40° inclination). V_C is the maximum cruise speed and V_{FE} is the maximum flaps extended speed of a Cessna Skyhawk.

[7] http://www.cessna.com/single-engine/skyhawk

5 Summary of results

5.1 Commercial aircraft: Engine ingestion

1. 3 out of 4 collisions are expected to result in ingestion of the UAV into one of the engines.
2. The loss of the engine should be assumed, with possible blade fragment throw.
3. UAV ingestion is very unlikely to result in a catastrophic outcome.

5.2 Commercial aircraft: Airframe

1. For a typical airframe aluminium skin (thickness: 1/8"—1/16"), penetration is predicted for velocities above 200kts, independent of UAV size (the lightest impactor weighing 67g).
2. During approach with fully extended flaps (at V_{FE}=160—180kts), penetration is predicted for a big UAV, and is very likely for a small UAV.
3. A single engine, fixed-wing UAV is predicted to penetrate the aluminium skin at velocities as low as 40—60kts.

5.3 Commercial aircraft: Windscreen

1. The results strongly depend on the material properties used in the model. The windscreen is likely to tolerate the impact of a small UAV without penetration at V_{FE}.
2. The likelihood of penetration from the impact of a big UAV remains unclear.
3. A fixed-wing UAV is predicted to penetrate the windscreen at velocities below V_{FE}.
4. The inclination of the windscreen reduces the normal forces, resulting in a higher impact resistance compared to the normal impact into the metal skin.

5.4 General aviation aircraft: Windscreen

1. Penetration is predicted at maximum cruise velocity (V_C=124kts for a Cessna 172), independent of UAV size.
2. Penetration is predicted for a big UAV at V_{FE} (87kts).
3. Penetration is unlikely for a small UAV at V_{FE}.

5.5 Conclusions

- A mid-air collision between a commercial airliner and an UAV is most likely to result in the ingestion of the UAV into one of the engines (3 out of 4 events). Reduction or loss of engine thrust with potential debris throw must be assumed. From past experience, engine loss and uncontained engine failure can be regarded as non-catastrophic events.
- A mid-air collision at impact velocities above 200kts is predicted to result in airframe skin penetration, independent of the UAV size. The consequences of such penetration will depend on the impact location.
- During the landing approach (at or below V_{FE}=160—180kts), a collision with a large UAV is likely to lead to skin and windshield penetration of a commercial airliner.
- A general aviation windscreen will be penetrated at cruise velocity. During approach (at or below V_{FE}=87kts), a large UAV will penetrate the windscreen; a small UAV is likely to be deflected without penetration.
- No experimental data exist to validate the predictions of windscreen penetration by a solid object. It is recommended to commission an experimental study, impacting actual UAV parts into common windscreen materials. Until then, the results presented in this report should be treated as rough estimates.

6 Appendix

A. The FAA penetration equation

The FAA penetration equation is based on the energy required to punch a round hole in a sheet of metal. It has been shown to give accurate, and conservative (Buyuk, et al., 2008) predictions during turbine fragment penetration tests (Lundin, 2001) (Lundin, 2002), and has been applied in a modified form in other studies (Wilde, 2010). The equation uses a combination of physics, an empirically derived constant C_S, and the following two assumptions:

1) The minimum energy required for penetration is equivalent to the energy required to shear out a "plug" of the impacted material, as illustrated in Figure 16.
2) The normal component of the impact velocity is the only source of kinetic energy relevant to the minimum energy required for penetration.

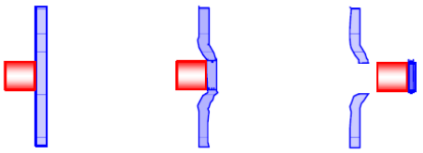

Figure 16: "Plug" penetration of a plate.

These assumptions lead to the following equation:

$$\frac{1}{2}m(V_{50}\cos\theta)^2 = C_s L t^2,$$

where the left hand side represents the kinetic energy of the projectile normal to the plate and the right hand side represents the mechanical work necessary to shear out a plug of the target material. Thus, the FAA equation for the ballistic limit V_{50} is:

$$V_{50} = \sqrt{\frac{2LC_S t^2}{m\cos^2\theta}}$$

where

- m = the mass of the projectile [kg]
- θ = the obliquity [radians]; see Figure 9
- C_S = an empirically determined shear constant [Pa], which is roughly correlated with classical material properties
- L = the perimeter of the subtended presented area of the projectile [m]: in the case of impacts with obliquity this is the area of the projectile normal to the velocity at impact and projected onto the target (e.g. roughly the perimeter of the hole in the target)
- t = the thickness of the target material [m].

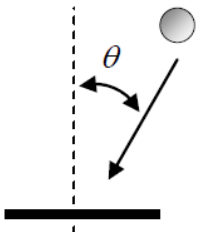

Figure 17: Geometry of the oblique impact.

V_{50} is classically defined as the velocity where there is a 50% probability of penetration. Further details can be found in (Wilde, 2010). There are two major difficulties in applying the FAA equation:

The material properties of the target are combined in the shear constant C_S. This constant was determined empirically from ballistic impact tests on Aluminium and steel plates (Gunderson, 1977), which theoretically limits the applicability of this equation to these two materials. On the other hand, it has been noted by (Wilde, 2010) that this constant roughly correlates with classical material properties. This implies that the material's shear strength (sometimes referred to as 'Static Yield

Limit') can be used as a good approximation for C_S; for aluminium: 210—290MPa, depending on the alloy. This fact was applied in this report for impacts into Lexan windscreens; the shear strength of Lexan was used for C_S.

The second difficulty lies in calculation of the impact area perimeter. The underlying assumption of the FAA equation is that certain energy is required to shear out a plug along the perimeter of the impact area. The longer this shear line in the material is, the more shearing energy is needed. It is obvious, that the orientation of the impactor relative to the target plate will determine the impact area and perimeter. Figure 18 shows the presented area A_P of an irregularly shaped object onto a surface perpendicular to the flight path. To calculate the shear line in the target plate which is oblique to the flight path vector, the area A_P must be projected on the inclined surface and its perimeter calculated. This requires the prior knowledge of the impactor orientation and its flight path (impact velocity vector) relative to the target plate.

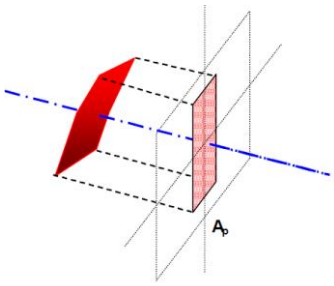

Figure 18: Presented area along the flight path.

In the present study, the orientation of the impacting UAV parts relative to the aircraft surface is not known. One possibility would be to assume the worst-case (smallest impact area) and best-case (largest impact area) scenarios. Yet, the associated areas do not have equal probability, and the worst-case scenario is likely to be over-restrictive. To accommodate all possible impact orientations, a probabilistic approach has been chosen, in which a pre-defined impactor geometry (battery, motor…) is rotated about all three axis, and its projection on the target surface is calculated. In case of the windscreen, a 40° inclination of this surface relative to the flight path of the object is added. The perimeter of this projected area is calculated for each impact orientation, which leads to a probability distribution. The results show that the worst-case scenario is the least likely, and that the most probable perimeter is almost twice as large as the smallest. The details of the MatLab simulation can be found in Appendix B.

The distribution of probability for a certain impact perimeter (and the derived ballistic limit V_{50}) is represented in form of a boxplot (sometimes called box-and-whiskers plot). A boxplot graphically depicts a set of numerical data through their quartiles (Figure 19). A quartile contains a quarter (25%) of all data points of the set. The upper and lower whisker ends show the maximum/minimum values; the central box combines 50% of all data points. The line in the box shows the median. The boxplot should be interpreted as follows: If the box lies half-way between the whiskers and has approximately the same length as the whiskers combined, then the data is uniformly distributed. Figure 19**Error! Reference source not found.** shows a data set concentrated and skewed to higher values, as the main box is considerably smaller than the whiskers and lies closer to the maximum value. In the present study, this would mean that higher values are more likely; the V_{50} velocity should be expected to lie close the maximum value, and smaller values are less probable.

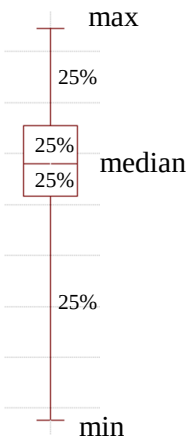

Figure 19: Box plot

The boxplot should not be confused with an error bar plot. The boxplot shows the variability of the result due to only one parameter (impact area perimeter L). The errors and uncertainties in the remaining parameters of the FAA equation are not accounted for.

An objection to the probabilistic approach is the fact that UAV components are installed with a 'standard' orientation (motors vertically, battery pack usually horizontally), which makes their orientation pre-determined relative to the horizontal plane during hovering and slow level flight. Nevertheless, such assumptions would limit the scope of impact possibilities and, in particular, exclude the worst-case scenario ('tail-on' impact with the smallest area). The probabilistic approach, on the other hand, provides an overview of the whole range of possibilities, regardless of the design of the particular UAV model.

B. Monte Carlo simulation

To compute the probability distribution of the impact perimeter L for the FAA equation, surface meshes of two geometric objects were created in MatLab: A square blocks, representing the UAV battery pack and the camera payload; and a cylinder, representing the UAV electric motor (Figure 20). The projection of these surface meshes onto a flat surface (inclined by 40°, in case of the windscreen) provided the impact area and perimeter length. The object was rotated in steps of 8° (45 steps per 360° rotation) about all three axes, resulting in $45^3 = 91125$ projections per object. A histogram of the perimeter lengths for a sample case is shown in Figure 21. The strong skewness of the distribution towards the maximum value implies that a small-area impact (a 'tail-on' collision) is least likely. The cumulative sum (blue line) is used for the calculation of the quartiles and the boxplot. The boxplot reflects the strong skewness towards large perimeters by having the main box and the median located at the right end of the range (see insert in Figure 21).

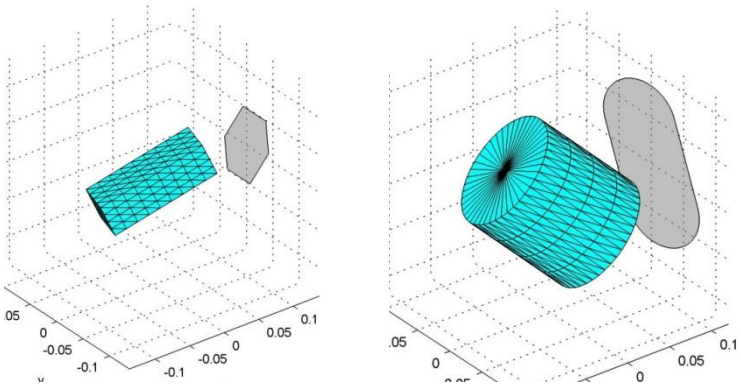

Figure 20: 3D mesh and its projection for the battery pack (left) and motor (right).

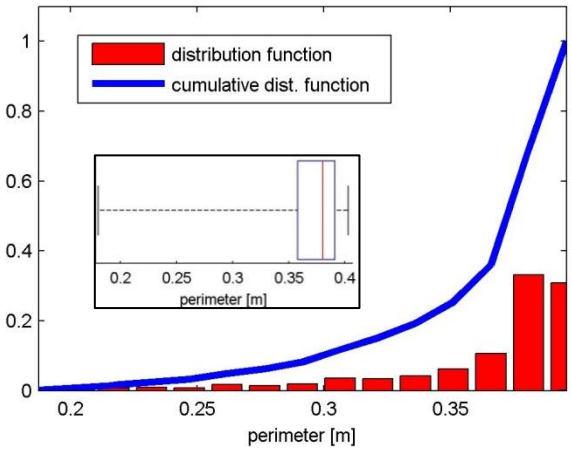

Figure 21: Impact perimeter distribution for a battery pack (red bars) and the cumulative distribution function (blue line) for the calculation of statistics. The resulting boxplot is shown in the insert. The data show a strong skewness to large impact perimeters, making 'tail-on' collisions least likely.

C. Mathematical discussion of probability

The three-dimensional object impacting an inclined surface is a very complex problem for an analytical probabilistic treatment. The underlying mathematical principles can be explored analytically when this three degrees of freedom problem (3DOF) is reduced to a 1DOF situation.

The simplest problem to consider is the projection of a unit line (length=1) onto a wall perpendicular to the horizontal axis, as shown in Figure 22. The line is fully determined by only one parameter, the angle α. The length of the projection will be termed *X*, with:

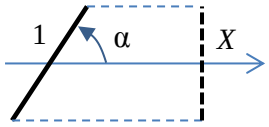

Figure 22: Projection of a line of length 1.

$$X = |\sin\alpha|$$

X is periodic with α, and the full range of results is reproduced within $0 \leq \alpha \leq \pi/2$ ($0 \leq \alpha \leq 90°$). When considering probabilities, we can say that the continuous *sample space* Ω consists of lines of lengths between 0 and 1, with *X* being the *continuous random variable*, which describes the outcome of a random experiment (Grinstead & Snell, n.d.). The 'experiments' consist of picking α randomly between 0 and $\pi/2$ many times, and calculating *X*. The result is a distribution of probabilities for a certain outcome. This can be represented in form of the *cumulative distribution function* $F(x)$, which describes the probability *P* that the outcome *X* will lie below a given value *x* (in this case $0 \leq x \leq 1$):

$$F(x) = P(X \leq x)$$

With $X = \sin\alpha$, we can write:

$$\begin{aligned} F(x) &= P(\sin\alpha \leq x) \\ &= P(\alpha \leq \sin^{-1} x) \\ F(x) &= \frac{2}{\pi}\sin^{-1} x \end{aligned}$$

The step leading to the last equation can be understood from Figure 23: The probability for $\alpha \leq \sin^{-1} x$ at a given x_i is equivalent to the ratio of the red to green lines.

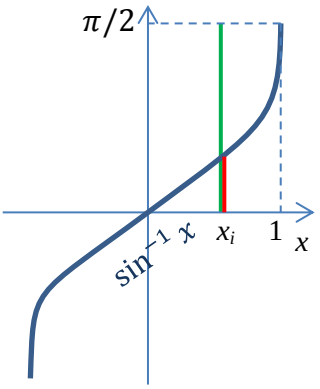

Figure 23: Geometric representation of the probability of $\alpha \leq \sin^{-1} x$.

The *probability density function* $f(x)$ is computed as:

$$f(x) = \frac{dF(x)}{dx} = \frac{2/\pi}{\sqrt{1-x^2}}$$

These functions are plotted in Figure 24, which shows that the probability density is far from uniform, and is concentrated at larger values of *x*. This means that it is more likely to encounter values close to 1 than to 0. This is quantified by the quartiles (0.25, 0.5, 0.75) plotted as crosses in Figure 24, with the larger cross representing the median of the distribution. The median lies at 0.707, meaning that in 50% of all 'experiments', the length *X* will lie below this value, and in 50% above. Low values of *X* are less likely: for example, the probability of encountering the smallest 10% of all projection lengths is only 6.3%, compared to a probability of 28.7% for the highest 10%.

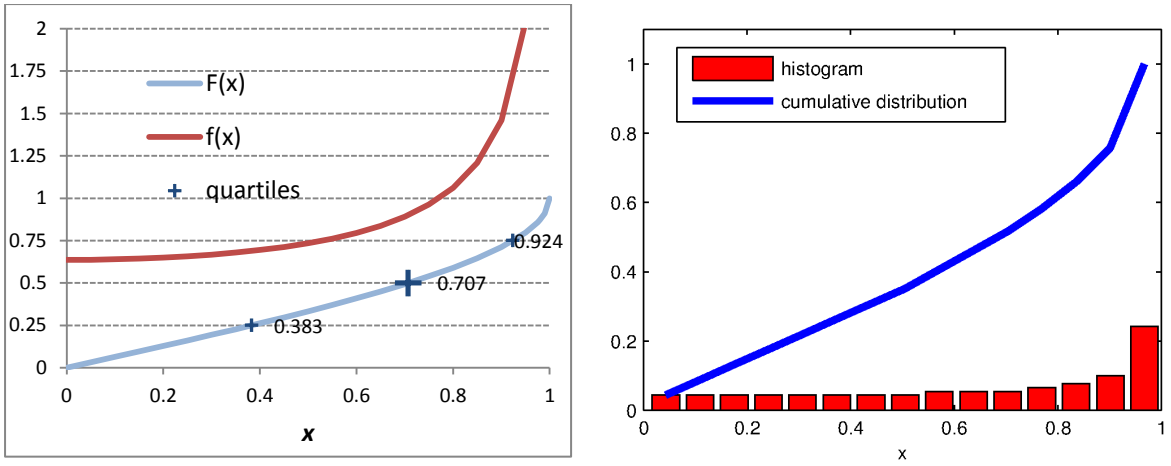

Figure 24: Cumulative distribution function F(x) and probability density function f(x) of the projection length. Left: Analytical solution; right: MatLab simulation.

This probability distribution explains why it is so difficult to make a knife stick with its pointy end in a soft target by throwing it with a spin. As it has been shown, it is more likely that it will impact with its long side than with its pointy end.

When transferring these results to the 3DOF case of an elongated three-dimensional object impacting the windscreen, it is apparent that the impactor is more likely to present a large impact area/perimeter. The worst-case scenario, the object impacting with its smallest surface, is less likely.

7 Bibliography

ATKINS, 2008. *Bird Strike Damage & Windshield Bird Strike - Final Report,* s.l.: European Aviation Safety Agency.

Buyuk, M., Loikkanen, M. & Kan, C.-D., 2008. *Explicit Finite Element Analysis of 2024-T3/T351 Aluminum Material Under Impact Loading for Airplane Engine Containment and Fragment Shielding,* Washington, DC: U.S. Department of Transportation (Federal Aviation Administration).

Cleary, E. C., Dolbeer, R. A. & Wright, S. E., 2006. *Wildlife Strikes to Civil Aircraft in the United States 1990-2005,* s.l.: Bird Strike Committee.

Cole, K. J., Young, L. W. & Jordan-Culler, T., 1997. *Hazards of Falling Debris to People, Aircraft, and Watercraft,* Albuquerque, New Mexico: Sandia National Laboratories.

Draper, C. H. & Wilde, P. D., 2008. *Development of a Business Jet Class Survivability Model for.* Honolulu, Hawaii, AIAA 2008-7122.

Goldsmith, W., 1999. Non-ideal projectile impact on targets. *International Journal of Impact Engineering,* Volume 22, pp. 95-395.

Grinstead, C. M. & Snell, L. J., n.d. *Introduction to Probability.* 2nd ed. s.l.:American Mathematical Society.

Gunderson, C., 1977. *Study to improve airframe turbine engine rotor blade containment,* s.l.: U.S. Department of Transportation.

Lundin, S., 2001. *Engine Debris Fuselage Penetration Testing Phase I,* s.l.: U.S. Department of Transportation.

Lundin, S., 2002. *Engine Debris Fuselage Penetration Testing Phase II,* s.l.: U.S. Department of Transportation.

RCC, 2007. *Common Risk Criteria Standards for National Test Rdanges: Supplement,* New Mexico: Range Commanders Council, U.S. Army White Sands Missile Range.

Smojver, I. & Ivancevic, D., 2011. Bird strike damage analysis in aircraft structures using Abaqus/Explicit and coupled rian Lagrangian approach. *Composites Science and Technology,* Volume 71, p. 489–498.

Thorpe, J., 2012. *100 years of fatalities and destroyed civil aircraft due to bird strikes.* Stavanger, Norway, International Bird Strike Committee 30/WP.

Vignjevic, R., Olowski, M., De Vuyst, T. & Campbell, J. C., 2013. A parametric study of bird strike on engine blades. *International Journal of Impact Engineering,* Volume 60, pp. 44-57.

Wilde, P. D., 2010. *Aircraft Protection Standards and Implementation Guidelines for Range Safety.* Orlando, Florida, AIAA 2010-1542.